COMPUTATIONAL STUDIES OF GRAPHENE AND SILICENE FOR DNA BASE DETECTION

A Thesis by

MUKESH TUMBAPO

Submitted to the Jackson College of Graduate Studies of the
University of Central Oklahoma
in partial fulfillment of the requirements for the degree of
MASTER OF SCIENCE

Chair of Committee:

Dr. Benjamin O. Tayo

Committee Members:

Dr. Weldon J. Wilson

Dr. Yuhao Jiang

Chair of Department

Charles Hughes

December 2020

Major Subject: Engineering Physics-Physics

COMPUTATIONAL STUDIES OF GRAPHENE AND SILICENE FOR DNA BASE DETECTION

Mukesh Tumbapo

APPROVED:

Thesis Advisor Benjamin O. Tayo

Dr. Benjamin O. Tayo, Engineering & Physics Department

Committee Chair Benjamin O. Tayo

Dr. Benjamin O. Tayo, Engineering & Physics Department

Committee Member Weldon J. Wilson

Dr. Weldon J. Wilson, Engineering & Physics Department

Committee Member Yuhao Jiang

Dr. Yuhao Jiang, Engineering & Physics Department

COMPUTATIONAL STUDIES OF GRAPHENE AND SILICENE FOR DNA BASE DETECTION

An abstract of the thesis by

Mukesh Tumbapo

Graphene's success for nanopore DNA sequencing has shown that it is possible to explore other potential single- and few-atom thick layers of elemental 2D materials beyond graphene (e.g. phosphorene and silicene), and also that these materials can exhibit fascinating and technologically useful properties for DNA base detection that are superior to those of graphene. The buckled honeycomb structure, tunable bandgap, and high thermal stability of silicene makes it an ideal material that can be used for designing the active components of nanodevices for biosensing applications such rapid sequencing of DNA. Additionally, the tunable bandgap of silicene provides versatile electronic and thermal properties allowing silicene to be tuned into both a semi-metallic material and a semiconducting material. Due to the remarkable properties of silicene, it is therefore extremely important to perform exploratory studies to determine silicene's ability to detect individual DNA bases as this material is being sought after by many experimental groups as a promising alternative to graphene for designing nano-bioelectronic devices for high-speed DNA sequencing. In this thesis, using density functional theory (DFT), we studied the interaction of DNA bases with finite-size nanomaterials from silicene and graphene. To determine the potential of monolayer silicene as a DNA sensing material, we performed first-principal calculations based on two device concepts, namely, nanoribbon and nanopore devices. Due to the differences in structural and electronic properties of DNA bases, each base is expected to have a unique interaction with the silicene, or graphene monolayer material and this interaction was modeled and quantified using density functional theory. In this research, we found that silicene devices have lower binding energies compared to graphene devices, reflecting the minimal sticking of DNA

bases to silicene's surface in the optimized structures. We noticed a significant change in bandgap for DNA bases using silicene nanopore device compared to graphene devices. Furthermore, the silicene devices with DNA bases show a greater change in density of state signal compared to graphene. We also observed that the silicene nanopore device performs better than the graphene nanopore device. These findings support the idea of silicene being a potential candidate material for advanced DNA base detection using the transverse tunneling current modality. We hope that the findings of this research will provide useful insights that can serve as a guidance to experimentalists and material scientists working in the field. Ideas for future research include examining this system using a periodic calculation; simulate a real device and calculate the current spectrum; and expanding the research to include other single-layer materials such as transition-metal dichalcogenides, and Van der Waals heterostructures.

ACKNOWLEDGEMENT

With all my heart, I want to say many thanks to my thesis supervisor, Dr Benjamin O. Tayo, for his encouragement and support in my education. His energy and interest inspired me to explore the realm of computational physics. I have been honored with the opportunity to work with him on this project. I would like to mention my classmate Matthew B. Henry, we collaborated a lot on this research project and he was always there to share and exchange ideas. Thanks to the HPC center for all the help and support with Buddy supercomputer. I would also like to thank my committee members Dr. Weldon Wilson and Dr. Yuhao Jiang for their support and guidance during the realization of this thesis.

Many thanks also to my entire family members for all their support on my pursuit of education. My sincere gratitude also goes to Sapana Gurung, my girlfriend for all her advice, financial support and words of encouragement during desperate times. I would also like to thank all my teachers and instructors, you each contributed to my academic journey and to you all I say many thanks, and may God bless you.

Thanks also go to my colleagues and friends, and the department faculty and staff for making my time at the University of Central Oklahoma a wonderful experience.

Above all, I want to thank God Almighty for His infinite love, wisdom, grace.

CONTRIBUTORS AND FUNDING SOURCES

Contributors

This work was supervised by a thesis committee consisting of Dr. Benjamin O. Tayo [Advisor], Dr. Weldon Wilson and Dr. Yuhao Jiang of the Department of Engineering and Physics at the University of Central Oklahoma.

Funding Sources

This research was funded by the RCSA grant.

TABLE OF CONTENTS

LIST OF TABLES

LIST OF FIGURES

LIST OF ABBRIBRIATIONS

DNA – DEOXYRIBO NUCLEIC ACID

RNA - RIBO NUCLEIC ACID

2D - TWO DIMENSIONAL

DFT - DENSITY FUNCTIONAL THEORY

HOMO - HIGHEST OCCUPIED MOLECULE ORBITAL

LUMO - LOWEST UNOCCUPIED MOLECULE ORBITAL

GNP - GRAPHENE NANOPORE

GNR - GRAPHENE NANORIBBON

SNP - SILICENE NANOPORE

SNR - SILICENE NANORIBBON

OPT GEOM - OPTIMIZATION GEOMETRY

B3LYP - BECKE, 3 - PARAMETER, LEE – YANG - PARR

DOS - DENSITY OF STATES

COD - CRYSTALLOGRAPHY OPEN DATABASE

CIF - CRYSTALLOGRAPHIC INFORMATION FILE

ssDNA - SINGLE-STRANDED DNA

hBN - HEXAGONAL BORON NITRIDE

MoS_2 - MOLYBDEUM DISULFIDE

6-31G (d,p) - GAUSSIAN BASIS SET WITH POLARIZATION FUNCTIONS

E_F - FERMI ENERGY

CHAPTER 1

INTRODUCTION

The vital and important genetic information hidden within the sequence of bases in DNA has caused a high demand of fast and cost friendly DNA sequencing methods. The ability to sequence the DNA is expected to help in the diagnosis and treatment of various diseases and eventually for revolutionization of personalized medicine[1][2]. In search of cost friendly methods, nano devices (for e.g. nanopores and nanoribbons) from various materials have been intensely studied with the goal of finding the best material than can be used for cost-effective and rapid DNA sequencing. Starting a few decades ago, nanopore based sequencing methods were first introduced by Kasianowicz et al[3] with the use of biological nanopores such as the $\boldsymbol{\alpha}$-hemolysin protein pore inserted into a lipid membrane. While tremendous success in the field of single-molecule analysis was accomplished with biological nanopores, they suffer from several challenges that limit their use for single-base detection: 1) biological nanopores are very sensitive to temperature, PH, and applied voltage, making them unsuitable for practical applications[4], 2) most biological nanopores such as α-hemolysin are typically more than 10 – 20 nm thick (which is equivalent to about 30 – 60 DNA bases) [5], which makes it difficult to detect individual bases-specific modulation in ion currents or transverse tunneling currents as multiple base pairs interact with the pore/gap simultaneously [5][6]. Due to the disadvantage of biological nanopores, a second generation of nanopores emerged. These are called solid-state nanopores. Solid-state nanopores fabricated on membranes such as Si_3N_4 [7], SiO_2 [8], Al_2O_3 [9], and plastic [10] have been extensively used for DNA sequencing. For example, nanopores in silicon nitride membranes have been used to distinguish single- and double-stranded DNA (dsDNA) [11], and different polynucleotides [12]; and were able to detect DNA folding [13]. Furthermore, solid-state

nanopores have also been shown to detect proteins [14] and have been used to elucidate the dynamics of protein folding [15]–[17], as well as extract the protein's shape in real-time [18]. While solid state nanopores are advantageous over biological nanopores in terms of stability and robustness, they are too thick (10 – 20 nm) which makes single-base detection impossible. Furthermore, the fast speed of DNA translocation (10^7 bases/s in solid-state nanopores) makes single-base resolution using ionic currents challenging [19].

The emergence of ultrathin two-dimensional (2D) crystals such as graphene and transition metal dichalcogenides (TMDs) over the past two decades [19]–[21] has created new opportunities and potentials in the field of nanopore DNA sequencing. The single-layer nature of 2D materials is comparable to the size of the DNA base [20]–[22]. Hence these materials show strong promise to provide the necessary resolution at the single-base level [23], [24]. Graphene nanopores and nanogaps have been successfully used for DNA sequencing [25], [26]. While the single-layer nature of graphene provides the optimal thickness (0.34 nm) for single-base resolution [20], the major hindrance is the hydrophobic nature of graphene's surface. Because of the strong π-π interactions between graphene and the DNA, bases stick its surface [27], [28] leading to a significant reduction in translocation speed due to pore clogging [29]. Furthermore, the coexistence of different bases on the surface and pore makes single-base discrimination difficult [29]. Another issue is the problem of orientational fluctuations of nucleobases during DNA translocation through a graphene nanopore. This can give rise to overlapping current contributions from different bases [28]. It has been shown that the ionic blockade signal shows noise for DNA translocation through a single-layer graphene nanopore [28]. The origin of this noise has been attributed to the atomic thickness of the pore. It is notable that a nanopore in a three-layer graphite structure, which has a thickness ~1 nm, shows a better signal-to-noise ratio (SNR) [28]–[30]. The

lack of a bandgap in pristine graphene makes it undesirable for use in electronic-based detection modalities such as tunneling current or field-effect transistors (FETs) [19].

With all the disadvantages of graphene nanopores, most efforts have recently focused on 2D materials beyond graphene. Among these, MoS_2 is the most widely studied for sequencing applications, mainly due to the ease of fabrication of MoS_2 devices [22], [31], [32]. Several theoretical and experimental studies have demonstrated sequencing using single-layer nanopores of MoS_2 [31], [33]–[35]. These studies reveal that MoS_2 performs better than graphene. For instance, improved SNR, non-stickiness of DNA to MoS_2 surface, and the presence of an intrinsic bandgap makes it suitable for use in advanced sequencing devices such as FETs [19], [31]. WS_2 has also been investigated for sensing properties and it showed properties similar to MoS_2 [1]. Hexagonal boron (hBN) has also been explored as an alternative to graphene[36], [37].

The field of nanopore sequencing using 2D materials has already witnessed tremendous success. While single-base detection has been realized using these materials, most of the studies performed so far were based on probing ionic current variations caused by the blocking of nanopore by different bases during DNA translocation. The ionic current method is capable of achieving single-base resolution only at low translocation speeds due to low bandwidth for recording ionic current [31], [38]. Also, to the best of our knowledge, among the large family of 2D materials, only graphene, hBN, MoS_2, and WS_2 have been investigated for DNA sequencing [31]. At this stage, it is not clear what solid-state nanopore material will be able to meet the challenges for single-base resolution. Thus, it is critical to continue to carry out explorative studies to identify new nanopore materials that could potentially emerge as the best candidate material.

This signifies the need for exploration of different 2D materials beyond graphene. This research will focus on a promising elemental 2D crystal called silicene. The goal of this project is to perform computational studies on silicene nanomaterials with the purpose of quantifying it's ability for detecting DNA bases using advanced detection principles such as tunneling current or field-effect transistor device. The buckled honeycomb lattice of silicene, large tunable bandgap, and single atom thickness makes silicene to be a potential alternative to graphene for high speed DNA sequencing and it is expected to bring new opportunities into the field of single-molecule analysis using 2D materials.

Most of the research performed for DNA base detection using graphene was based on probing ionic current blockade signal. But due to the atomic thickness of 2D materials, it has been shown that ionic current blockade signal shows noise for DNA translocation through a single layer graphene nanopore[31][39]. Since the thickness of monolayer silicene is comparable to that of graphene, one would expect similar noise levels in the ionic current signal for silicene as well. However, silicene's direct bandgap of 1.194 to 1.979 eV [40], allows us to focus on advanced detection concepts such as the transverse tunneling current method which probes electronic current as opposed to ionic current, and hence expected to produce a higher signal-to-noise ratio. As sequencing by tunneling current has been achieved using solid state pores[41], [42], this method is therefore a viable option worth further exploration for silicene as well. The thickness of silicene may cause noise in ionic blockade signal but the important aspect of these atomic thick layers (<1 nm) is, it allows us to perform sequencing at single base resolution. Whereas other 2D material such as MoS_2, WS_2, hBN have larger thicknesses (≅ 1 nm) as compare to silicene (≅ 0.29 nm), which is very close to the thickness of DNA bases (0.35 nm). The other major issue with graphene nanopore based detection was sticking of bases on the edges of pore during the translocation

process, complicating the tunneling current signal and making the detection of individual bases to be difficult. So, developing a device that can hold the base firmly without sticking is beneficial rather than engineering non sticky pore in graphene itself[31][8], [43], [44].

In a typical nanopore device experiment, single stranded DNA (ssDNA) or RNA molecules are driven electrophoretically through a nanopore (1 to 2 nm wide) created in a 2D material. During translocation, the DNA nucleobases with the pore, thus modulating the transverse tunneling current, as shown in Figure 1. The tunneling current is expected to change with each base due to the change in the structural and electronic properties of each base[1][45][46].

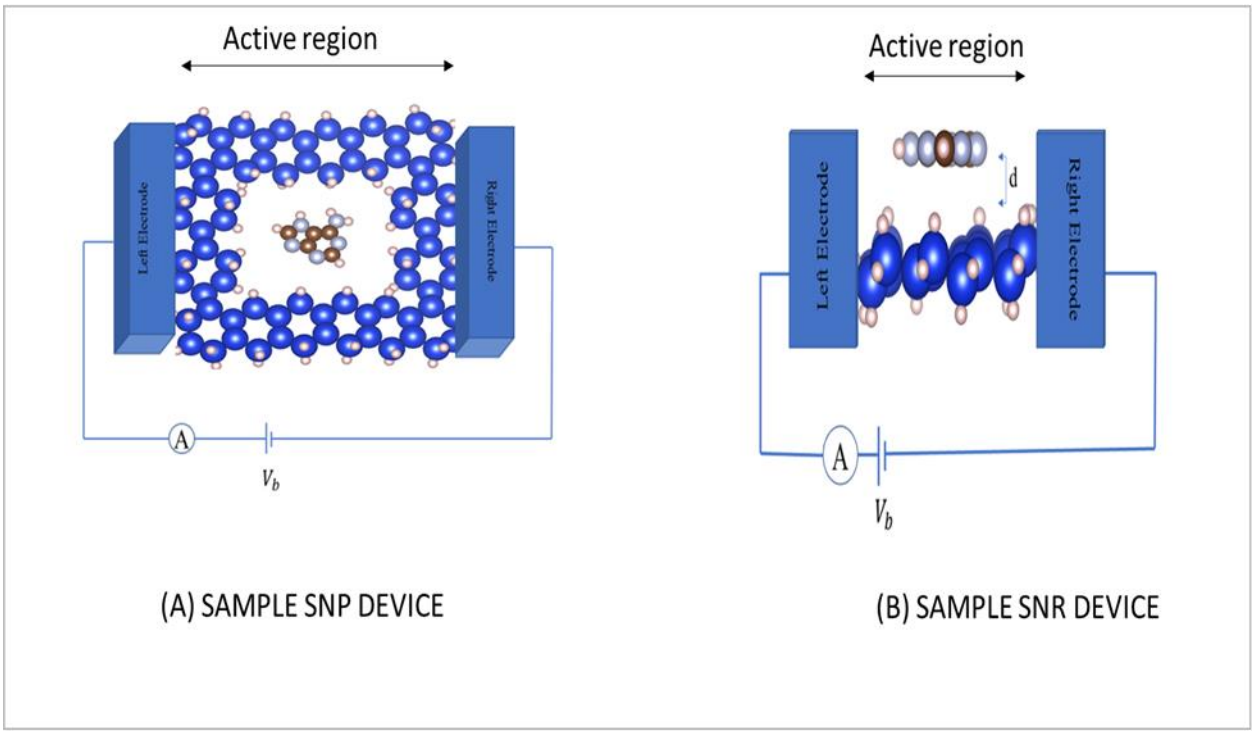

Figure 1: Diagram showing the sample model of SNP and SNR device.

Another device principle is based on modulation of transverse current due to physisorption of DNA bases on the surface of nanoribbons from 2D materials, as shown in Figure 1.

In this research instead of modeling the entire ssDNA (which is computationally very expensive for electronic-based first-principle calculations), we modeled the interaction of individual DNA bases with the corresponding 2D nanomaterial. This approach mimics the interaction of bases with nanopore or nanoribbon during a translocation or physisorption experiment and has been used in several computational studies. Using density functional theory simulations, we will model and study the interaction of DNA bases with nanopore and nanoribbon structures from silicene. To evaluate the performance of our 2D systems for DNA base identification using the tunneling current effect, we shall calculate three important device performance metrics, namely, the binding energy, bandgap, and density of states [28][33][45]. We shall compare our results with graphene, which is the most widely studied 2D material for DNA sequencing applications.

This thesis is organized as follows. In chapter 2, we discuss about DNA sequencing principles. In chapter 3, we discuss several two-dimensional materials that could be used for DNA base detection. In Chapter 4, we present an overview of density functional theory and the computational methods used in our studies. In Chapter 5, we studied the interaction of graphene nanomaterials with DNA bases. In Chapter 6, we studied the interaction of silicene nanomaterials with DNA bases. In Chapter 7, we present a summary of the thesis, conclusions, and perspectives.

CHAPTER 2

DNA SEQUENCING PRINCIPLES

DNA sequencing is the method to sequence the nucleobases within the DNA. There are four nucleobases in DNA, that is Adenine, Cytosine, Guanine and Thymine. The pattern of these bases is believed to carry all the genetic information and DNA sequencing helps to decode this information. This information further helps to understand the functioning of genes and helps to detect certain genetic changes that can lead to various health conditions, for instance cancer induction. The ability to sequence the DNA in a fast and cost effective manner is therefore an important technological problem whose solution can serve as a game changer in the diagnosis and treatment of certain genetic diseases, and subsequently in personalized medicine.

Several theoretical and computational studies have been performed by different research groups to evaluate the potential of 2D materials as candidate materials for rapid and high-resolution sequencing of the DNA. Most of these studies were based on the detection of ionic current modulations during DNA translocation through a nanopore created in a 2D material. The major drawback with the ionic current method is the low signal to noise ration which makes the identification of individual bases to be very difficult. Recently, much effort has been focused on using advanced detection methods that probe electronic current, as opposed to ionic current [33]. Electronic-based detection methods are believed to produce signal to noise ratios that are stronger and less susceptible to orientational fluctuations of DNA bases during tunneling. Two of the most widely studied electronic-based detection methods are transverse current modulations due to interaction of DNA bases with nanopore during DNA translocation [28], [33], and transverse current modulations due to physisorption of DNA bases on the surface of nanoribbons from various 2D materials[45].

In this research, we will focus on using DFT to model and study the interaction of DNA bases with nanopores and nanoribbons from graphene and silicene. We shall use the results from graphene to benchmark of silicene studies, since graphene is the most widely studied 2D materials for DNA sequencing applications.

A model of silicene nanopore (SNP) and silicene nanoribbon (SNR) device concepts is shown in figure 1. It consists of left and right electrodes connecting in a circuit, where the applied bias voltage (V_b) will create an electric field and that will cause the motion of electrons in the active region of the device. Due to the physical gap in the nanopore (Figure 1a), the transport of electrons through the pore is governed by quantum tunneling. For the physisorption device concept (Figure 1b), the transverse current flowing through the nanoribbon is modulated by interaction of different DNA bases with nanoribbon surface. Thus, when the nanoribbon wide is made very small (comparable to interbase distance within the DNA), spatial resolution of DNA bases can be achieved by measuring the distinct current signal produced by each base.

In this research instead of modeling the whole device, we will mostly focus on the active region and study the interactions of SNP and SNR in presence of different bases. Based on changes of bandgap, binding energy and density of states (DOS), a clear understanding of the interaction is made, and a criterion for detection is evaluated. For instance, we will show later that the DOS is a direct measure of the tunneling current, since the tunneling current is proportional to the DOS. Also, the binding energy provides valuable information to quantify the strength of interaction between DNA bases and nanopore or nanoribbon. The greater the binding energy, the greater the ability of the bases to stick to the nanopore or nanoribbon surface, which could then lead to a noisy signal and decrease in speed of translocation.

2.1 DNA

DNA (deoxyribonucleic acid) is a molecule composed of two polynucleotide chains that coils around each other to form a double helix structure. This structure carries the genetic information from one offspring to another, such as instructions for development, growth, functioning, reproduction etc. The two polynucleotides chains are composed of simpler monomeric units called nucleotides. Nucleotides are composed of one of four nucleobases (Adenine, Cytosine, Thymine, Guanine), a sugar and a phosphate group[46]. Nucleotides form covalent bonds with one another (linking the sugar molecule of one and the phosphate group of the other) and creates a chain like structure giving rise to the sugar-phosphate backbone of the DNA[47]. The nucleobases from one strand are bound together with those of the other strand by hydrogen bonding interactions in a complimentary base-pair arrangement(Adenine bonds with Thymine and Cytosine bonds with Guanine), which runs in opposite direction forming a double helix structure. It is the sequence of nucleobases along the backbone that encodes the genetic information and DNA sequencing is the technique of determining the sequence of these nucleic acids in the DNA structure. The molecular geometries of the four nucleobases in a DNA molecule are shown in Figure 2.

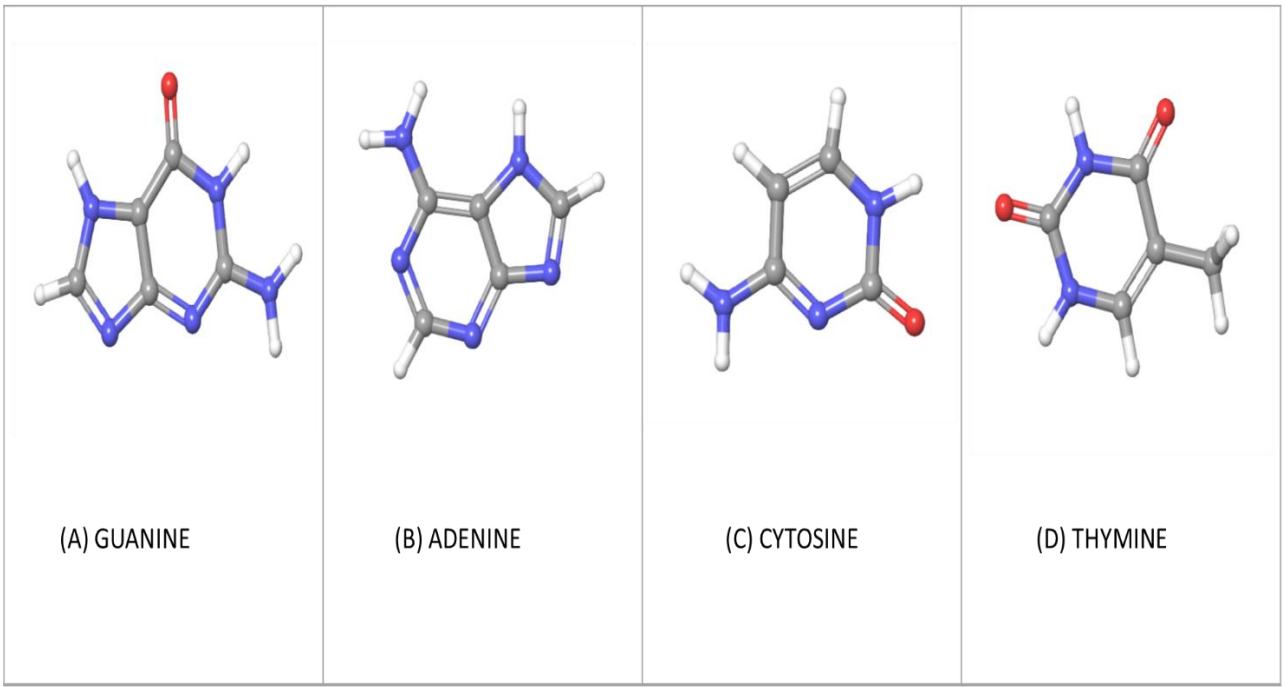

Figure 2: Four different types of DNA bases (a) Guanine, (b) Adenine, (c) Cytosine, (d) Thymine. The white solid spheres represents the hydrogen atom, grey for the carbon atom, red for oxygen atom and blue for nitrogen atom.

To decode this information, we perform computational studies using density functional theory to study the interaction of nucleobases with nanomaterials from monolayer graphene and silicene. For this purpose, we will perform electron base detection which probes modulations in the transverse tunneling current due to interaction of the channel (graphene and silicene) with the different nucleobases. The detection of electron tunneling current is a quantum phenomenon and is believed to produce enhanced signal to noise ratio compared to the ion-blockade method which probes the modulation of ionic current during translocation of DNA through nanopore and is very susceptible to noise due to orientational fluctuations of nucleobases during translocation. In the tunneling method, electrons have a non-zero probability to tunnel through the single layer graphene and silicene channel material. Furthermore, the tunneling current is believed to be significantly modulated as a result of interaction of the silicene with the different bases[48].

The structure of DNA bases is shown in Figure 2. From Figure 2, we can see the structure of bases are different from each other and they are likely to interact differently with nanopores and nanoribbon from single-layer silicene and graphene.

2.2 IMPORTANCE OF DNA SEQUENCING

DNA sequencing plays a pivotal role in mapping out the human genome. This information helps to understand the functioning of genes, and any alterations that could be induced to the genes. . The primary purpose of sequencing one's genome is to obtain information of medical value for future care. It can provide genetic variants which leads to disease or can increase the risk of disease development, even in asymptomatic people[1]. The solution to DNA sequencing could lead to cost effective methods that could, in turn, produce advancement in the field of genomics and personalized medicine(pharmacogenomics)[2].

CHAPTER 3

TWO DIMENSIONAL MATERIALS

Two-dimensional (2D) materials are often referred to as single layer materials. They have a single layer of atoms expanding in two-dimension giving rise to a large surface area and atomic-size thickness. This unique property of 2D-materials make them ideal materials for studying the adsorption of biomolecules on their surface via π-π stacking. The ultrathin nature and other unique properties such as high electrical conductivity, tunable optoelectronic properties, and high mobility shows the possibility of advanced sensing device application [25]. Additionally, the single layer nature of 2D materials is comparable to the size of DNA base (0.34nm) and hence these materials have the potential to produce the necessary resolution at the single base level. A list of some of the 2D materials with their thickness is shown in the Table 1. The thickness of these 2D materials seem to vary, only the well-known graphene seems to have fixed thickness, but as these materials are considered one atomic thick layer, the diameter of atom is considered as the thickness of these 2D materials.

2D- materials	Strucutre	Thickness(Å)	Buckling distance(Δ) (Å)	Bond length (Å)
Graphene	honeycomb	3.350	0.000	1.420
Silicene	buckled honeycomb	2.940	0.450	2.350
Germanene	buckled honeycomb	4.220	0.737	2.460
Phosphorene	puckered honeycomb	2.8 ± 1.5 nm (2–7 layers)	0.300	2.11–2.43

Table 1: Thickness and shape of some elemental 2D-materials[49-51].

There has been lots of research interest in exploring the potential of using 2D-materials for DNA sequencing. Most of the research conducted so far were mostly based on graphene. Due to the strong interaction of graphene with DNA bases, bases stick on graphene surface or graphene nanopore due to π – π interactions, leading to a significant reduction in translocation speed and

pore-clogging. Also the coexistence of different bases on the surface and pore makes single-base detection difficult [1][8]. Furthermore, the overlapping current contributions from different bases, and lack of bandgap in pristine graphene makes it undesirable for use in electronic base detection. This signifies the need of extending these studies to other elemental 2D materials [25]. This research will focus on exploring the potential of silicene as a DNA sequencing material[49]. We shall benchmark our results by comparing silicene to graphene as it is the most widely studied material for DNA sequencing. For each of these sensing materials, we will perform a comprehensive computational study based on two main detection principles:

1. Modulations of tunneling current through nanopore created in 2D material in the presence of the different DNA bases.

2. Changes in 2D membrane current due to the physisorption of DNA bases onto the surface of the 2D material.

In this research, instead of calculating the current directly, we shall compute density of states from the output of our DFT calculations. As shown in Eq. (1), the tunneling current is proportional to the density of states [28]. Hence any changes in the density of state is likely to result in changes in the tunneling current. So, we will calculate the density of state plot for all the device systems in the presence of different DNA bases. This would enable us to quantify the changes in 2D materials properties induced by its interaction with the different DNA bases. The tunneling current can be modelled using this equation,

$$I(E, V_b) = \frac{e}{\pi\hbar}\int_0^E dÉ\ DOS(E - É) \tag{1}$$

Here, DOS is the density of state, I is the current, E the energy and V_b the applied bias voltage.

CHAPTER 4

DFT AND COMPUTATIONAL METHODS

DFT stands for density functional theory. It is a computational modeling method used for studying the electronic structure of atoms, molecules, polymers, nanostructures and crystals [50]. The hypothesis behind the DFT is to use a physically observable quantity (electron density) that allows us to construct the Hamiltonian of the system and then use it to solve for ground state wave function and energy levels of the system. In 1964, Pierre Hohenberg and Walter Kohn put forth the first firm theoretical framework of DFT signifying that all information in a system is contained in the physically observable quantity , that is, the 'electron density', which is a simple function of three coordinates. The electron density which minimizes the total energy for a given system is the ground state electron density, according to the variational principle.

4.1 IMPLIFICATION OF DENSITY FUNCTIONAL THEORY

Density functional theory is a computational quantum mechanical model for solving the Schrodinger wave equation for many body systems (systems consisting of nuclei and electrons). The numerical implementation of DFT is made possible by the Born-Oppenheimer approximation. Under this approximation, the nuclei and electronic degrees of freedom can be separated (this approximation is justifiable because the nuclear mass is thousands of times larger than the electronic mass, which means electron kinetic energies are thousands of times larger than nuclear kinetic energies). This allows us to express the total wave function of the system as a product of the electronic and nuclear wave functions. The electronic Schrodinger equation can then be solved while keeping the nuclei fixed. The calculated ground state electronic energy (which depends on the nuclear coordinates) is then used to compute the nuclear potential energy, from which the forces acting on each nucleus can be computed. Without the Born-Oppenheimer approximation,

the implementation of DFT would be impossible (except for very small molecules) even with the use of powerful supercomputers .

A simple diagram illustrating the geometry optimization process and calculation of molecular energy levels using DFT is shown in Figure 3. The geometry optimization process involves two main steps, the self-consistent field cycle, and the optimize cycle. The self-consistent field cycle start with an initial guess of the electron density, which is obtained from the initial geometry of molecule and the ground state atomic wave functions (orbitals) of all the atoms in the system. The initial electron density is then used to calculate the effective electronic potential energy (at fixed nuclear coordinates). The effective potential for the system is used to solve Schrodinger wave equation. A wavefunction obtained from the solution of Schrodinger wave equation is used to calculate the new electron density using Eq. (2).

$$\rho(\vec{r},\vec{R}) = \int \psi\,(\vec{r},\vec{f};\vec{R})^{*}\,\psi(\vec{r},\vec{f};\vec{R})\,d^{3}\vec{f} \tag{2}$$

where $\vec{f}$ represents the coordinates of the remaining (N-1) electrons, and $\vec{R}$ represents all the nuclear coordinates. This process is repeated until the electron density is converged. The converged energy of the system is then used in the optimize cycle to compute the forces on the nuclei. During the optimize cycle, the energy gradient or the total force is calculated by taking the gradient of the total energy, which is used to adjust the relative position vector for each atom. The process is repeated in a cyclic manner until the total force on each nuclei becomes negligible or less than threshold value (specified by the force convergence criterion) and thus the final optimized geometry is obtained for the molecular system.

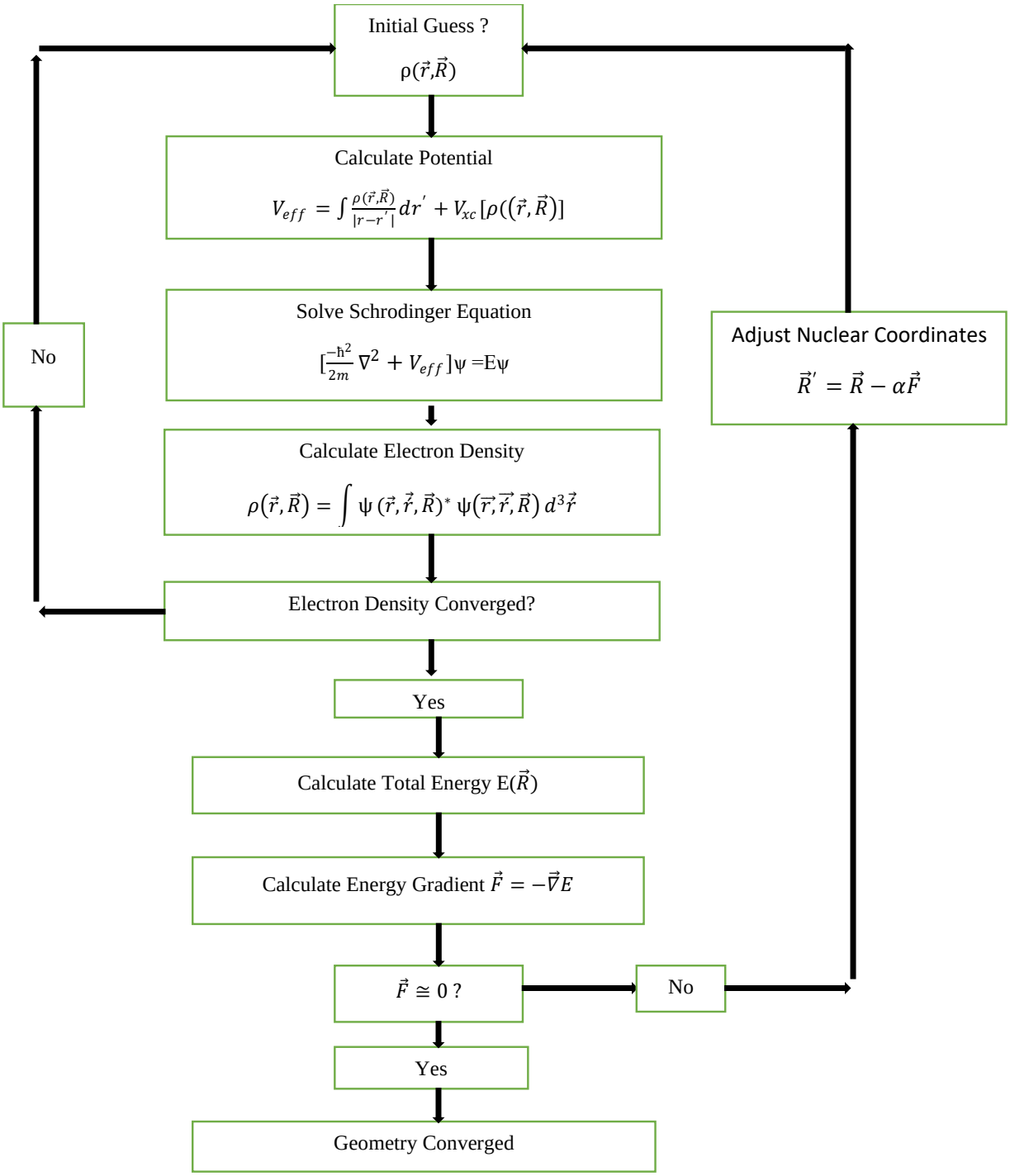

Figure 3: Flow chart illustrating the DFT process for computing equilibrium geometry and quantized energy levels of a system.

4.2 COMPUTAIONAL METHODS AND HPC/BUDDY

In condensed matter physics and materials sciences, computaional methods refer to the study of complex sytems by the means of computer simulations. These model are capable of harnessing high computing power for scientific research and enable the quantitative testing of competing theories. Results from these calcultions will provide useful insights that can serve as a guide to experimental researchers working in the field of DNA sequencing and allow to objectively compare competing theories of DNA sensing device using graphene and silicene. Also, computational research is relatively easy to conduct, is less expansive and works as a perfect base model to complement experimental research. In this research, we will use computational methods based on DFT to explore and analyze the capabalities of graphene and silicene for DNA sensing appllication. We will focus on two device concepts, namely, the nanopore and nanoribbion methods. DFT studies require large scale calculations and high-performance computing (HPC) resources. For example, a nanopore model of graphene with a base inside the pore has about 150 atoms. With the availability of super-computer 'Buddy' at University of Central Oklahoma, it is feasible to conduct DFT studies for many body systems for the purpose of research. A Supercomputer is acomputer with a high level of performance. 'Buddy' in our case is made up of multiple smaller computers that sit in racks one on top of another, it operates at 32 teraflops, or 32 trillion calculations per second. 'Buddy' allows multiple users to work simultaneously on large scale research problems. Buddy also supports research and education in computational sciences for students and, researchers across the state of Oklahoma.

4.3 MOLECULAR EDITORS AND DFT SOFTWARE

One of the main objective of this research is to explore the relm of computational research and develop computational skills. Justifying the objective, this research requires the knowledge and

ability to use different software and programming languages. Initially, molecular editors and visualizers such as Jmol, Avogadro, Nanotube modeler, Vesta, Macmolplot, and Maestro were used to import, build and edit molecular geometries. For example all the nucleo bases shown in figure 2 were extracted from the molecular database using Jmol software.The structures and CIF of graphene from Nanotube Modeler, and the CIF of silicene from the Crystallography Open Database (COD). Molecular geometries were edited using Avogadro, Nanotube Modeler, Vesta, or Maestro. With the assistance from the HPC center of University, software like Filezilla, Putty were installed and used to remotely connect with Buddy supercomputer. Notepad ++ was used to edit and create batch scripts and for editing the input files used running calculations for different molecular structures.The final step is to perfrom the actual DFT calculations. There are many quantum chemistry and materials science software packages for running DFT calculations such as GAMESS, Gaussian, Quantum Espresso. Some of these are specialized for extended periodic systems or finite-size molecular systems. In our research, we will model the active component of the DNA sensing device as a nanosystem with finite size. Hence we shall use the Gaussian software package as it is the most popular and widely used DFT software for systems with finite size.

The Gaussian software is a computational chemistry software that can be used to model complex chemical reactions, predict molecular energies, model electronic structures, and much more advanced calcualtions based on fundamental principles of quantum mechanics with a good level of accuracy. Geometry optimization calculations were performed using the B3LYP potential energy model and the 6-31G (d,p) basis set approximation for atomic orbitals. In the optimization process, the atomic centers were relaxed until the force on each atom is less than 0.02 eV/Å. This

force convergence criterion is quite reasonable and allows the calculations to be completed within a reasonble time.

To illustrate how to run a geometry optimization calculation with the Gaussian software, we will consider the example of the DNA base Adenice. Starting with the XYZ file for Adenine (as shown in Figure 4a, the file was imported into the Avogadro software. A Gaussin input file was then generated using Avogadro as shown in Figure 4b. XYZ file simply contains the xyz coordinates of all atoms in any molecule or element. The first line in xyz file denotes the total number of atoms in the system, the second line is the title or name of the molecule. The rest of the content are the xyz coordinates of all atoms in the system. For the Gaussian input file in Figure 4b, the first line of code represents the B3LYP level of theory, 6-31G (d,p) is the basis set and Opt is a keyword for running a geometry optimization calculation. After generating the Gaussian input file, a batch script file is then created for allocating computing resources and for submitting the caculations to buddy. This batch script file works as an envolope for input file and commands to run accordingly with the instruction from input file. The Figure 4c is a screenshot of the batch script file Adenine.sh used for running calculations on Adenine molecule. The batch script file is used to allocate resources (such as number of nodes, number of CPUs, DFT software to use, memory requirements, wall time, etc.) to be used for running DFT calculations for any given system. The batch scipt file also has an excecutatble command that is used to launch the calculation, and this includes the name of the Gaussian input file (Adenine.com – highlighted in blue in the input file) for the system of interest. Increasing the number of nodes used in batch script seem to enhance the calculation, but due to some limitations on the computing resources, we were limited to a maximum of 3 nodes per job.

```
15
adenine
N          -1.94941        -0.50446        -0.00001
C          -1.30725        -1.69059        -0.00007
N          -0.00125        -1.93055        -0.00008
C           0.73945        -0.80683        -0.00005
N           2.12147        -0.73741        -0.00002
C           2.38696         0.54515         0.00003
N           1.27118         1.34737         0.00003
C           0.18350         0.48683        -0.00003
C          -1.21682         0.61552         0.00004
N          -1.88440         1.80554         0.00011
H          -1.95886        -2.56194        -0.00011
H           3.38093         0.97374         0.00004
H           1.27121         2.35491        -0.00001
H          -1.42033         2.69543         0.00021
H          -2.89101         1.77395         0.00016
```

Figure 4a: Screenshot of sample xyz file_(Adenine.xyz) of DNA base Adenine.

```
#n B3LYP/6-31G(d,p) Opt

 Title

0 1
N          -1.94941        -0.50446        -0.00001
C          -1.30725        -1.69059        -0.00007
N          -0.00125        -1.93055        -0.00008
C           0.73945        -0.80683        -0.00005
N           2.12147        -0.73741        -0.00002
C           2.38696         0.54515         0.00003
N           1.27118         1.34737         0.00003
C           0.18350         0.48683        -0.00003
C          -1.21682         0.61552         0.00004
N          -1.88440         1.80554         0.00011
H          -1.95886        -2.56194        -0.00011
H           3.38093         0.97374         0.00004
H           1.27121         2.35491        -0.00001
H          -1.42033         2.69543         0.00021
H          -2.89101         1.77395         0.00016
```

Figure 4b: Screenshot of sample gaussian input file (Adenine.com) for the DNA base Adenine.

```
#!/bin/bash
#SBATCH --job-name=g16
#SBATCH --nodes=2
#SBATCH --cpus-per-task=20
#SBATCH --output=g16-%j.out
#SBATCH --partition=nodes

### Of the batch options, it is only recommnded to change "--job-name", "--nodes", and
### "--output". Any other modifications may result in an error.

### It is only recommneded to change the input file in the Gaussian command. If needed
### more g16 options can be added.

#Load Gaussian module
module load Gaussian/g16

#Gaussian scratch directory.
export GAUSS_SCRDIR=/home/$USER/.gaustmp/$SLURM_JOBID
mkdir -p $GAUSS_SCRDIR

#Stop OpenMP from interfering with Gaussian's thread mechanism.
export OMP_NUM_THREADS=1

#Prepare node list for Linda
for n in `scontrol show hostname | sort -u`; do
  echo ${n}
done | paste -s -d, > snodes.$SLURM_JOBID

#Run Gaussian. It is recommended to only change the input file here. If needed you can
#raise the memory up to 60GB, but doing so may result in an error.
g16 -m=40gb -p=${SLURM_CPUS_PER_TASK} -w=`cat snodes.$SLURM_JOBID` Adenine.com

#Clean up nodes list
rm snodes.$SLURM_JOBID
```

Figure 4c: Screenshot of sample Gaussian batch script file(Adenine.sh) for Adenine.

4.4 DFT CALCULATIONS FOR DNA BASES

As demonstrated above, the DFT simulation of Adenine was followed by calculations on the other bases. All the criteria for the computation was kept constant, this allows us to compare the properties of bases such as bandgap, HOMO, LUMO and binding energy. A simple output data for all the bases were gathered and kept in Table 2. The bandgap was calculated using the Eq. (3).

Gaussian output for DNA bases [B3LYP 6-31(d,p)]				
Bases	Total energy(eV)	Homo(eV)	Lumo(eV)	Bandgap(eV)
Adenine	-12716.354	-6.070	-0.692	5.378
Cytosine	-10746.907	-6.142	-0.783	5.358
Guanine	-14763.926	-5.602	-0.514	5.088
Thymine	-12358.025	-6.569	-1.028	5.541

Table 2: Total energy, HOMO, LUMO, and bandgap for DNA bases using DFT.

We observe from Table 2 that Thymine has the largest bandgap, and Guanine the least, while Adenine and Cytosine have approximately the same bandgap.

$$E_{gap} = E_{HOMO} - E_{LUMO} \tag{3}$$

The HOMO state in Eq. (3) is highest occupied molecular orbital and the LUMO state is the lowest unoccupied molecular orbital. The bandgap energy is the minimum energy required to excite an electron from the HOMO state to the LUMO state. The bandgap is very critical for characterizing the electronic and optical properties of different materials [51].

CHAPTER 5

GRAPHENE

Graphene consist of a single-atom thick plane of carbon atoms, hence considered a 2D system. It is also an alloptrope of carbon. Bonding in graphene is formed by sp2 hybridization in carbon atoms. This gives rise to the formation of 3 in-plane σ-bonds (formed by hybridization of the 2s, 2px, and 2py carbon orbitals) and one π-bond formed by rem pz orbital, and perpendicular to the plane. Unlike the in-plane σ bonds, the π bonds overlap weakly, hence they are responsible for the electronic properties of graphene (high electrical conductivity and mobility). On the other hand, 3 σ-bonds give rise to the honeycomb lattice structure and stability of graphene. The physical properties of graphene include a carbon to carbon bond length of 0.142nm, a planar density of 0.77mg/m^2, an atomic thickness of 0.35nm, and a high transparency of 97.7% [52]. Graphene also has excellent electronic and optical properties such as high mobility, ballistic transport, width-dependent tunable bandgap, flexible, stretchable, excellent thermal and electrical conductivities [1]. Given the remarkable properties and ultra thin nature, graphene provides new opportunities for use as active component in nanodevices for DNA sequencing. For DNA sequencing using monolayer graphene, we will focus on two detection modalties, that is the nanopore device and the nanoribbon device. The basic theory of a sensing device is the expectation of modulations of tunneling current across the nanoribbon due to physisorption on DNA bases on the surface of the nanoribbon since each base interacts different with the nanonoribbon. Similarly, we can monitor changes in the in-plane due to translocation of DNA bases through the nanopore created in graphene.

To explore graphene as sequencing material, a DFT simulation is performed using the Gaussian software package and orbital energies were calculated. Using the output from the DFT calculation,

the bandgap is calculated using Eq. (3) and with the help of Eq. (4), the binding energy is calculated for the different systems.

$$E_{BE} = E_{System+base} - E_{System} - E_{base} \quad (4)$$

Here, E_{BE} is the binding energy for the system, $E_{system+base}$ is total energy of combined system for each base and system, E_{system} total energy of system, and E_{base} the total energy of the DNA base. All calculations were performed at the B3LYP + 6-31G (d,p) level of theory with a force convergence criterion of 0.02 eV/Å.

To compare and identify trends and pattern, charts were made for each systems with different bases. To better visualize the distribution of energy levels, the density of states (DOS) was plotted for each system. This is important because the tunneling current is proportional to the DOS (see Eq. (1)). The DOS can be computed using the Lorentzian function as:

$$DOS(E) = \sum_{i=0}^{N} \frac{\Gamma}{[\Gamma^2 + (E - E_i)^2]} \quad (5)$$

where E is the energy, E_i are the molecular energy levels obtained from the DFT calculation, and Γ is the linewidth of the Lorentzian spectral function. In our calculations, we used Γ = 25 meV as this corresponds to the linewidth at room temperature.

5.1 DNA SENSING USING GRAPHENE NANOPORE

A sample nanopore device model is shown in Figure 1. As already discussed, we will be focusing on active region of the device. This region consists of the graphene nanopore and the DNA base at the center of the pore. A DFT simulation is performed using the Gaussian software package to calculate the transverse tunneling effect. The theory behind it is the possiblity that the electron can

hop through the nanodistance between the GNP and DNA base and give rise to the transverse tunneling current. The current in our case is evaluated in terms of density of states.

Starting with the structure of graphene, a graphene sheet with 156 atoms and having dimensions of 19.96 nm by 17.87 nm (LxB) was constructed using the Nanotube Moduler software. It was then edited using the Maestro software and the pore was created in the middle, by deleteing the central carbon atoms. All the edges were terminated by adding Hydrogen atoms to take care of the dangling bonds on carbon atoms at the edges. After deleting carbon atoms to create the nanopore, the GNP created consists of 141 atoms and the pore has the size of 1.03 nm by 1.039 nm (LxB). Since the average size of DNA bases is about 0.7 nm, this pore is big enough to contain the bases and small enough to produce strong signals. This process is followed by DFT calculation using the Gaussian software. To visualize the changes in structure of GNP, we plotted the stucture before and after geometry optimization. Figure 5 shows the changes in GNP structure after optimization. It shows that the bonds on the atoms at the edges of the structure have been shrunked in the process of optimization and the planar structure is lost. This is due to the fact that during the optimization process, the atoms are relaxed to equilibrium and this creates additional strain on the bonds, especially at the edges.

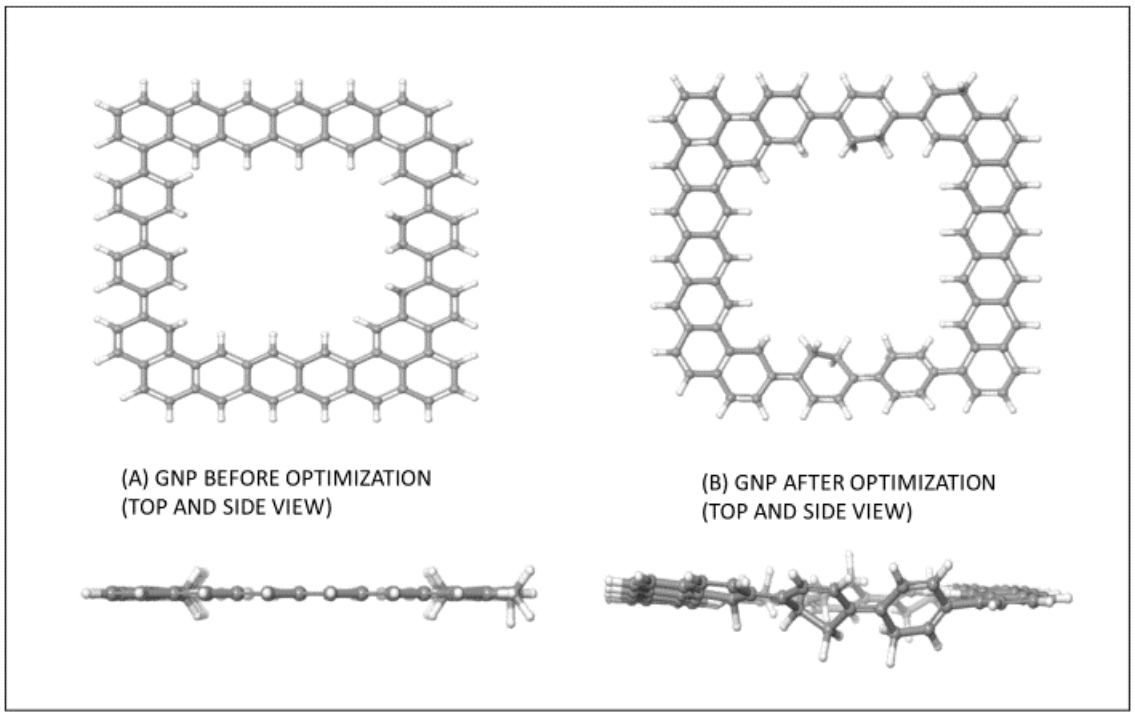

Figure 5: Structure of GNP before and after geometry optimization (grey color is for carbon atom and white for hydrogen).

From the simulation of Graphene nanopore, a HOMO energy of -3.94 eV, LUMO of -2.8947 eV and bandgap of 1.048 eV was obtained. These results are shown in Table 3.

Gaussian output for Graphene nanopore				
2d_elements	Total energy(eV)	Homo(eV)	Lumo(eV)	Bandgap(eV)
GNP	-89059.123	-3.943	-2.895	1.048

Table 3: Gaussian output for the pristine GNP.

To visualize the distribution of energy levels, a DOS plot is created for GNP. The DOS plot of GNP in figure 6 shows that GNP has a bandgap of 1.048 eV.

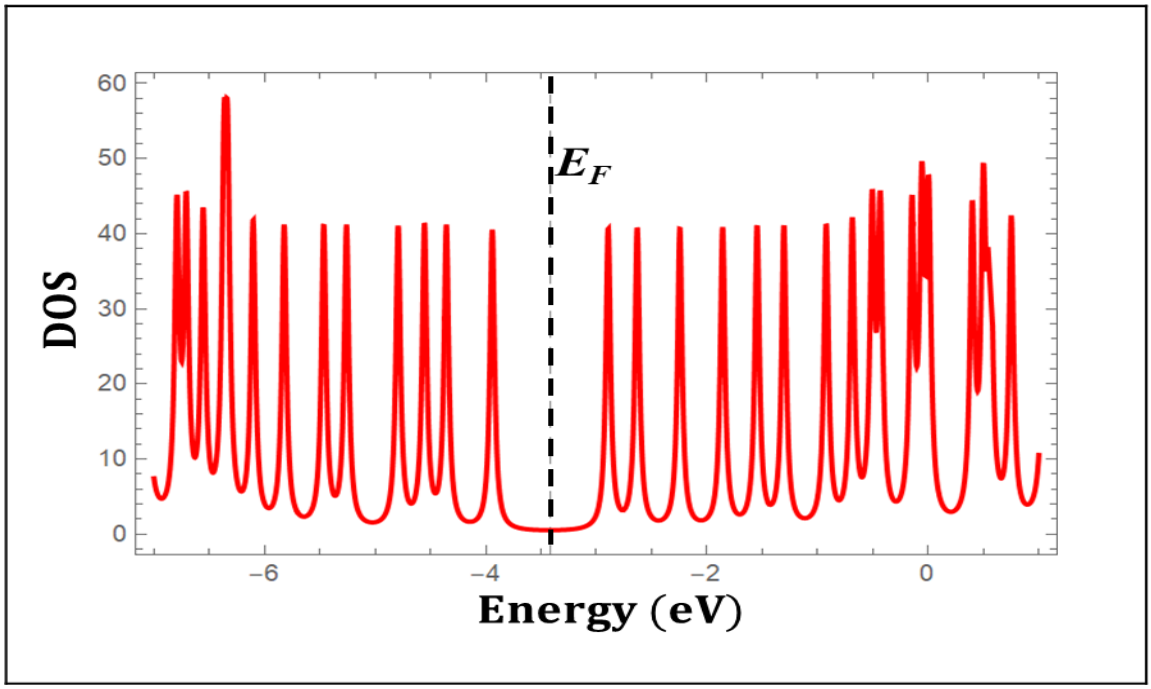

Figure 6: Plot of density of state for pristineGNP.The dotted line indicates the position of the Fermi energy level for pristine GNP.

After the initial calculation for pristine GNP, a combination of GNP with bases were created using the Maestro software and calculations with same criteria were performed using the Gaussian software. Figure 7 below shows the structures of GNP with different bases after the geometry optimization. It can be observed that after the optimization, nucleo bases tend to shift towards the edges of the GNP which could lead to the bases sticking on the surface and edges of the GNP, a well known problem with graphene devices [28]. In the case of GNP+A, GNP+C and GNP+T, the bases seems to be out of plane, and this could affect the reading of bases when the ssDNA translocates through the nanopore and this can produce error in the sequencing experiment.

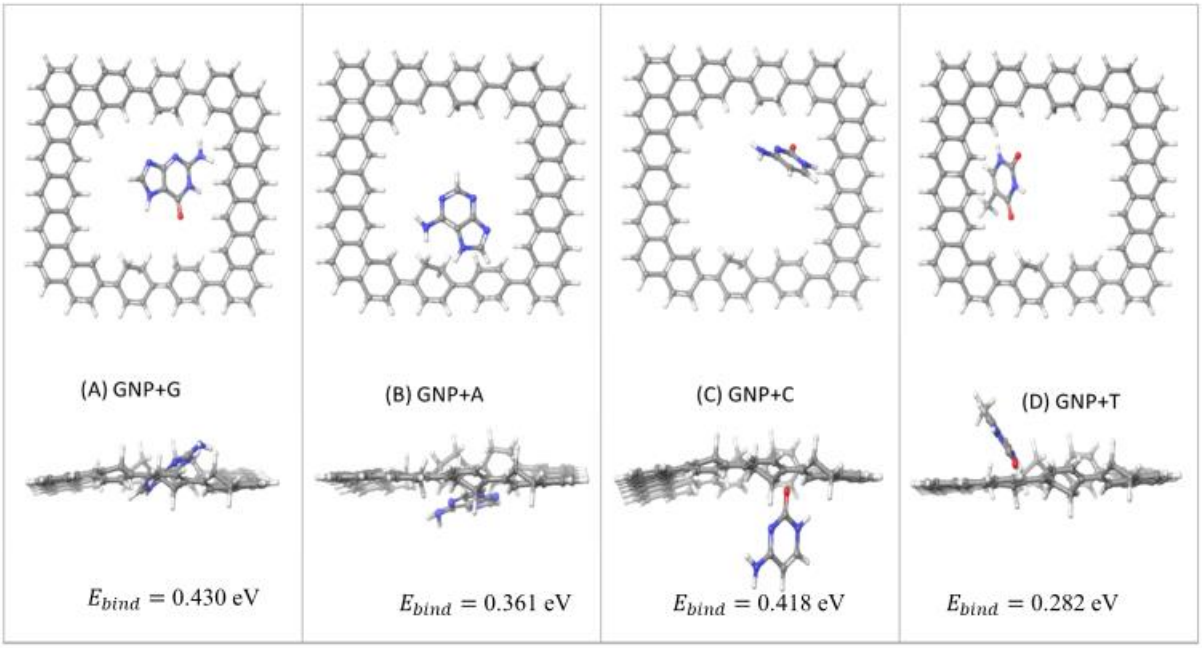

Figure 7: Optimized structures (top and side views) of GNP with different bases (grey color represent carbon atom, white for hydrogen, blue for nitrogen and red for oxygen).

The results from this section are summarized in Table 4.

DNA bases inside graphene nano pore [B3LYP 6-31(d,p)]					
combination	Total energy(eV)	Homo(eV)	Lumo(eV)	Bandgap(eV)	Binding energy(eV)
GNP+A	-101775.838	-3.901	-2.870	1.031	-0.361
GNP+C	-99806.448	-3.834	-2.746	1.088	-0.418
GNP+G	-103823.480	-3.918	-2.851	1.067	-0.430
GNP+T	-101417.430	-3.912	-2.862	1.049	-0.282

Table 4: Gaussian output for GNP+DNA bases (GNP +A for adenine, +C for cytosine, +G for guanine, +T for thymine).

It can be seen that bandgap for all the combination ranges from 1.03 eV to 1.09 eV. Among all, GNP+C has the highest bandgap of 1.087 eV and GNP+A has the lowest bandgap 1.031 eV. The binding energy gives the strength of interaction between bases and GNP. A binding energy range of 0.42eV to -0.28eV was obtained from the calculations. To further investigate the bandgap and

binding energy trend, we plotted the binding energy and bandgap for each base. In Figure 8, we can see that GNP+C stands out with highest energy gap and GNP+G with highest binding energy.

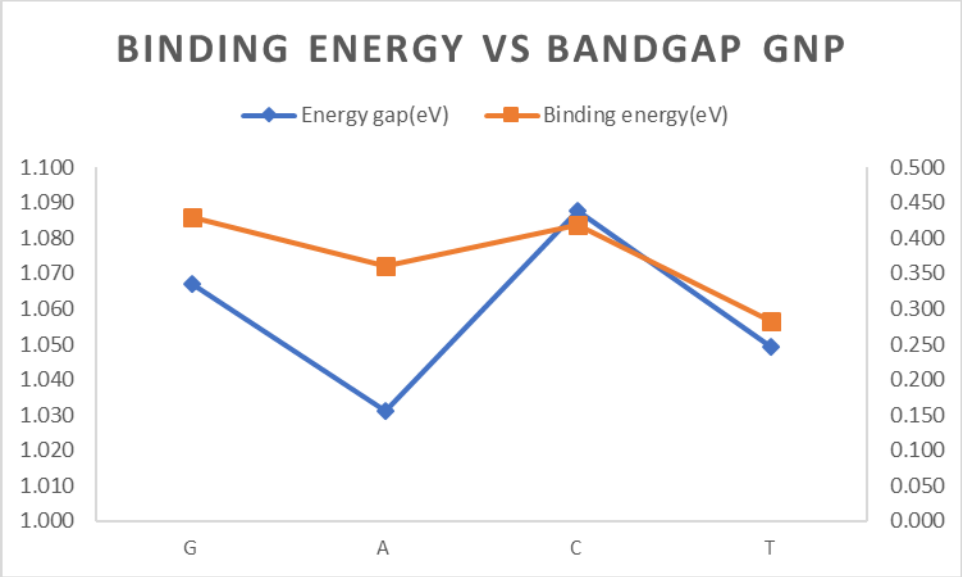

Figure 8: A chart comparing binding energy and bandgap of GNP+DNA bases.

Further, to visualize the possible transition of energy states, the density of state plots were made. Figure 9 shows the density of states for different combination of bases and GNP with respect to density of state for GNP is ploted. This plot will allow us to visualize the change occurred when the transition from GNP to GNP+bases is made. A fermi energy level for GNP is shown in dash line, it is calulate by taking average of homo and lumo state for GNP. Looking at the plot, it can be observed that there is slight change in density of state for graphene nanopore with bases inside in comparision to pristine GNP. This change in density of state signifies the change in current. So, definitely it can be said that there is change in interaction with the addition of bases inside the pore. Also the GNP+T has lowest binding energy resembiling weak interaction, GNP+G has the highest binding energy and GNP+A and GNP+C in the middle further proofs the different interactions or the tunneling effects.

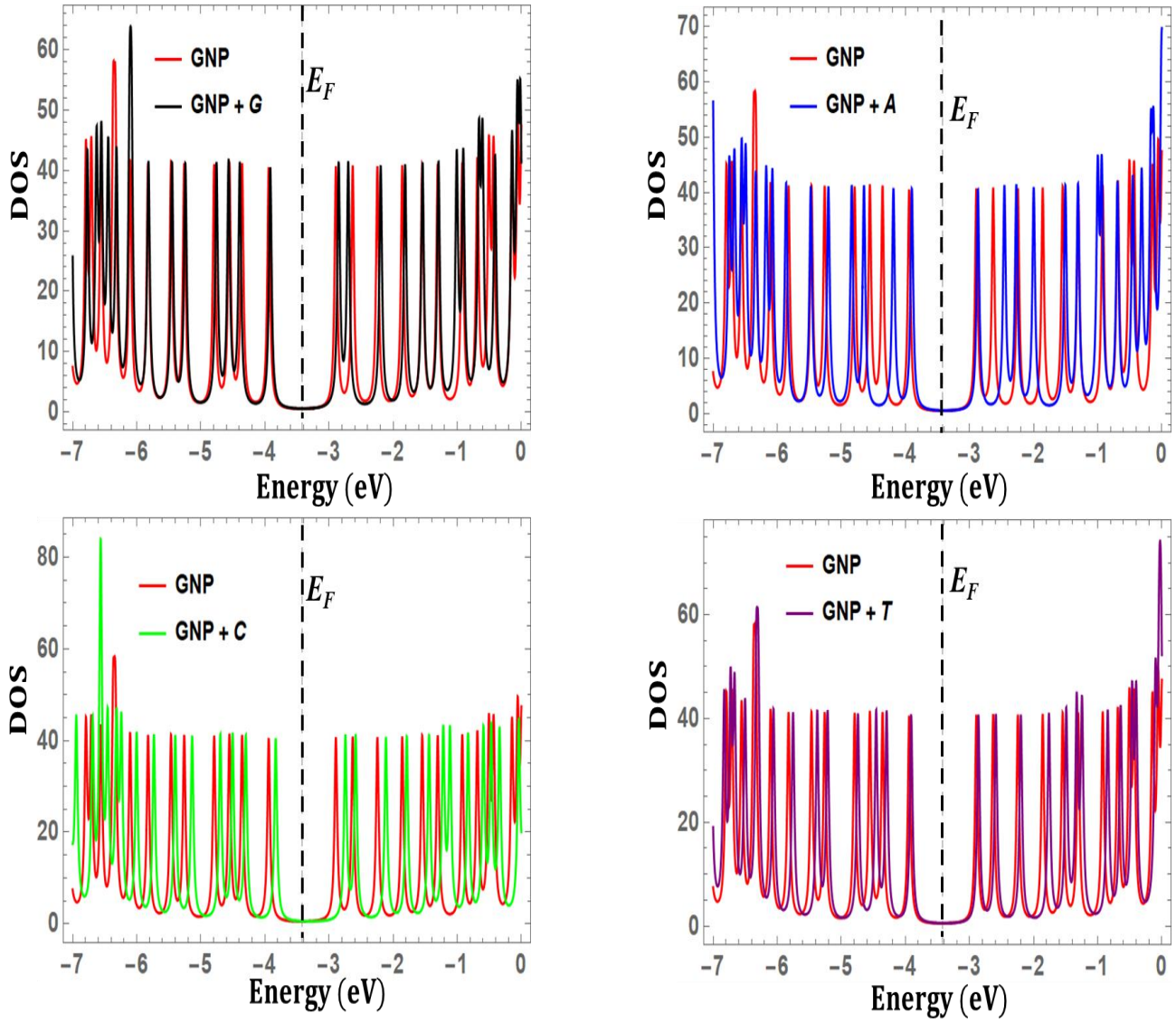

Figure 9: Plot of the density of states for DNA bases inside the GNP. The dotted lines indicate the positions of Fermi energy level for pristine GNP. We observe very small modulations in the DOS of the pristine GNP due to interaction with bases.

5.2 DNA SENSING USING GRAPHENE NANORIBBON (PHYSISORPTION)

A sample model of the GNR device is shown in Figure 1. In this process, the modulations of transverse current caused by physisorption of DNA bases onto the GNR surface is studied. For the purpose of this method, we created a single layer graphene sheet of dimensions 1.357 nm X 1.049 nm (LXB) with a total of 64 atoms. Similarly, as with the graphene nanopore, the edges of the GNR were terminated by adding hydrogen atoms. All the input parameters (such as model of potential energy, basis set, and force convergence criterion) for running the DFT calculations were kept constant for the GNP and GNR systems. The initial calculation for the pristine GNR gives a HOMO energy of -4.446 eV, a LUMO energy of -2.556 eV, and a bandgap of 1.891 eV, as shown on Table 5.

Gaussian output for Graphene nano ribbon (physisorption)				
2d_elements	Total energy(eV)	Homo(eV)	Lumo(eV)	Bandgap(eV)
GNR	-48001.312	-4.447	-2.556	1.891

Table 5: Gaussian outputs for pristine GNR system.

Figure 10 shows the structure of the GNR before and after the geometry optimization process. From Figure 10, no noticable changes can be observed between the two structures.

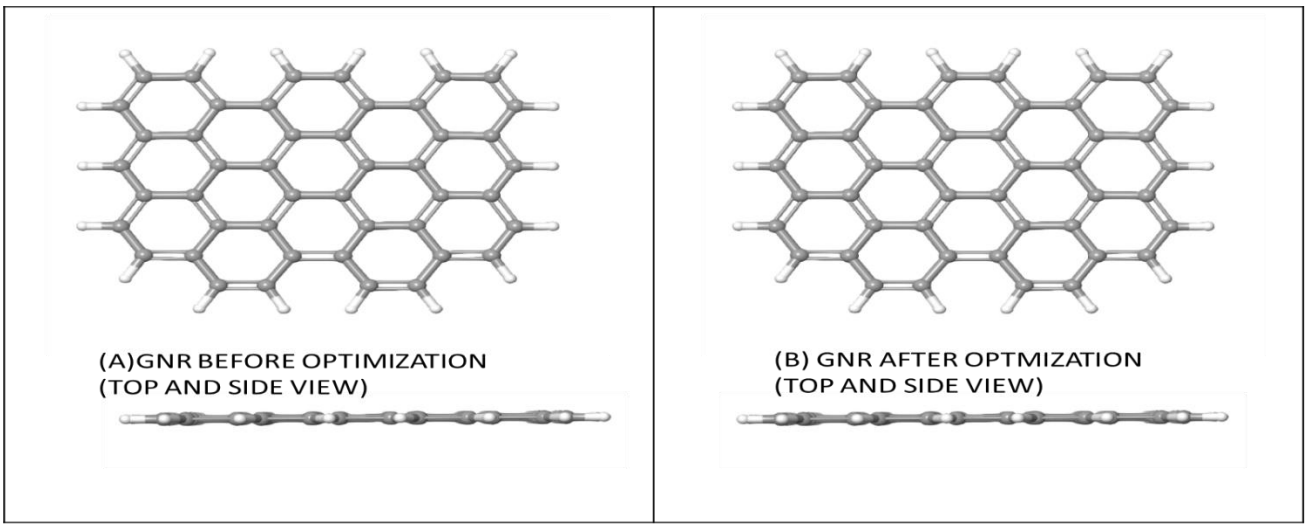

Figure 10: GNR before and after the optimization geometry calculation.

To visualize the distribution of energy levels, a density of plot is created as shown on Figure 11. The HOMO and LUMO states are identified and a bandgap of 1.891 eV can be observed in the plot.

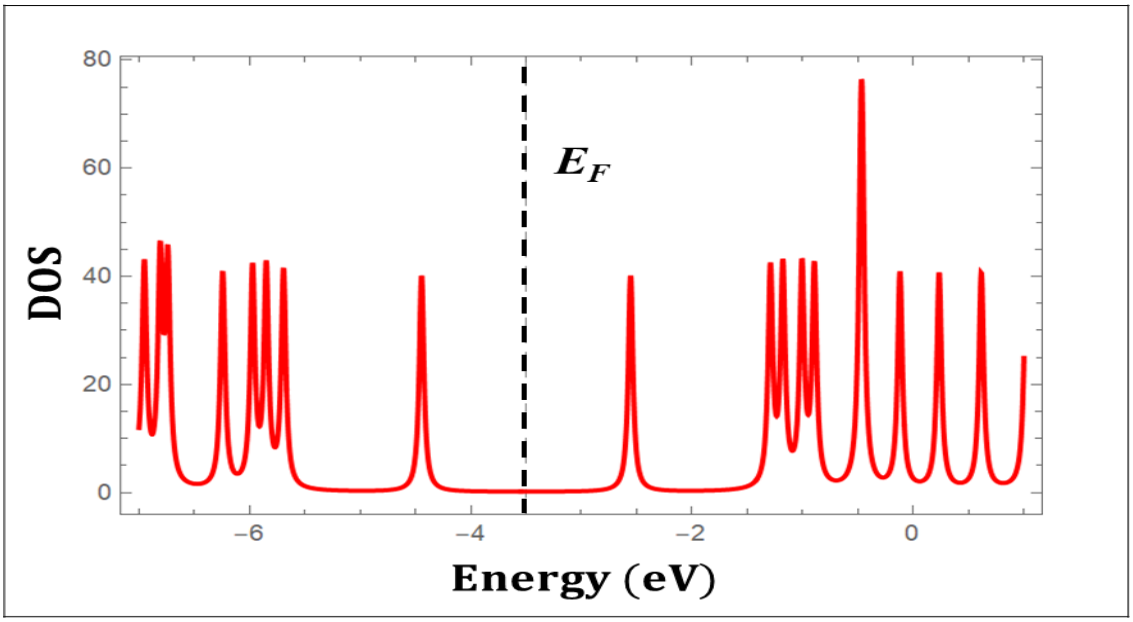

Figure 11: Plot of density of states for pristine GNR showing the bandgap. The dotted lines indicate the position of the Fermi energy level for pristine GNR.

Now after the initial calculations for the pristine GNR, the next step is to study the interaction of GNR with DNA bases. For this purpose, the DNA bases were placed above the surface of the optimized structure of GNR. The distance between the GNR and the DNA bases was adjusted to be 0.3 nm. The distance of 0.3 nm was choosen because we are interested in studying the process of physisorption (van der Waals interactions between base and GNR). If the bases are placed too close to the surface of the GNR, this would give rise to the formation of covalent bonds between the base and GNR. Sticking of bases on the surface of the surface of GNR is nonideal as this can significant decrease sequencing speed and produce errors in the read out as multiple bases interact with the GNR surface at any given time.

Gaussian output for Physisorption opt geometry B3LYP 6-31(d,p))					
Combination	Total energy(eV)	Homo(eV)	Lumo(eV)	Bandgap(eV)	binding energy(eV)
GNR+A	-60717.933	-4.798	-2.909	1.889	-0.267
GNR+C	-58748.526	-4.238	-2.356	1.882	-0.307
GNR+G	-62765.413	-4.594	-2.708	1.885	-0.175
GNR+T	-60359.568	-4.567	-2.677	1.890	-0.230

Table 6: A table showing the total energy, HOMO, LUMO, bandgap and binding energy of the GNR+DNA base systems.

Table 6 shows a summary of the results for all the calculations. The bandgap was observed to be in range of 1.882 eV to 1.89 eV, which is in range of 659 nm to 656 nm (in the wave length domain). The binding energy was more deviated from the range of 0.175 eV to 0.307 eV. To observe the relationship between the bandgap and binidng energy, a comparision chart is created.

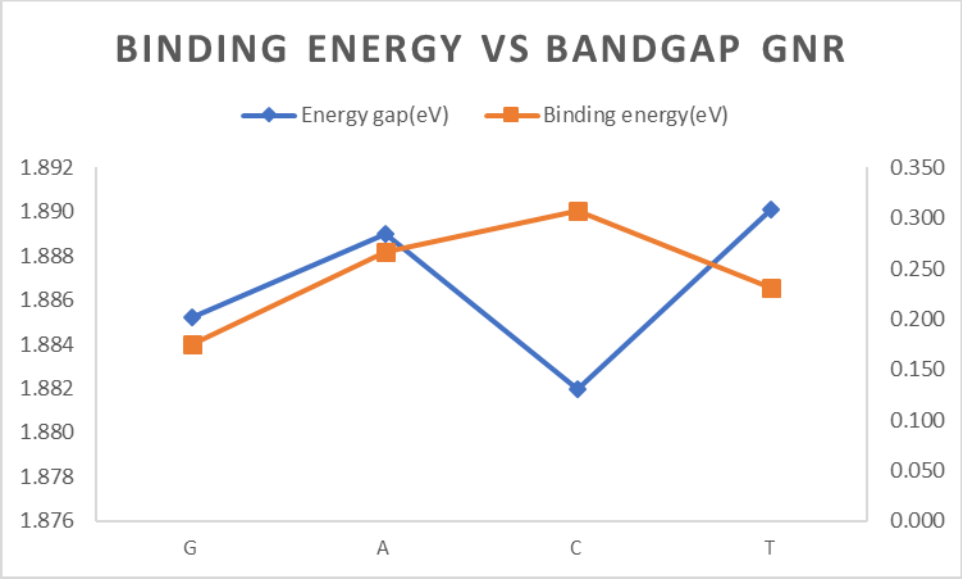

Figure 12: A chart comparing binding energy and bandgap of GNR+DNA bases.

On the chart on Figure 12, only GNR+C shows a distinct difference in bandgap and binding energy and distinguishable to rest of system. Generally, the modulations in the bandgap of the GNR due to physisorption of the DNA bases is very small. This shows that graphene is typically not a very good material for use in DNA sequencing by physisorption.

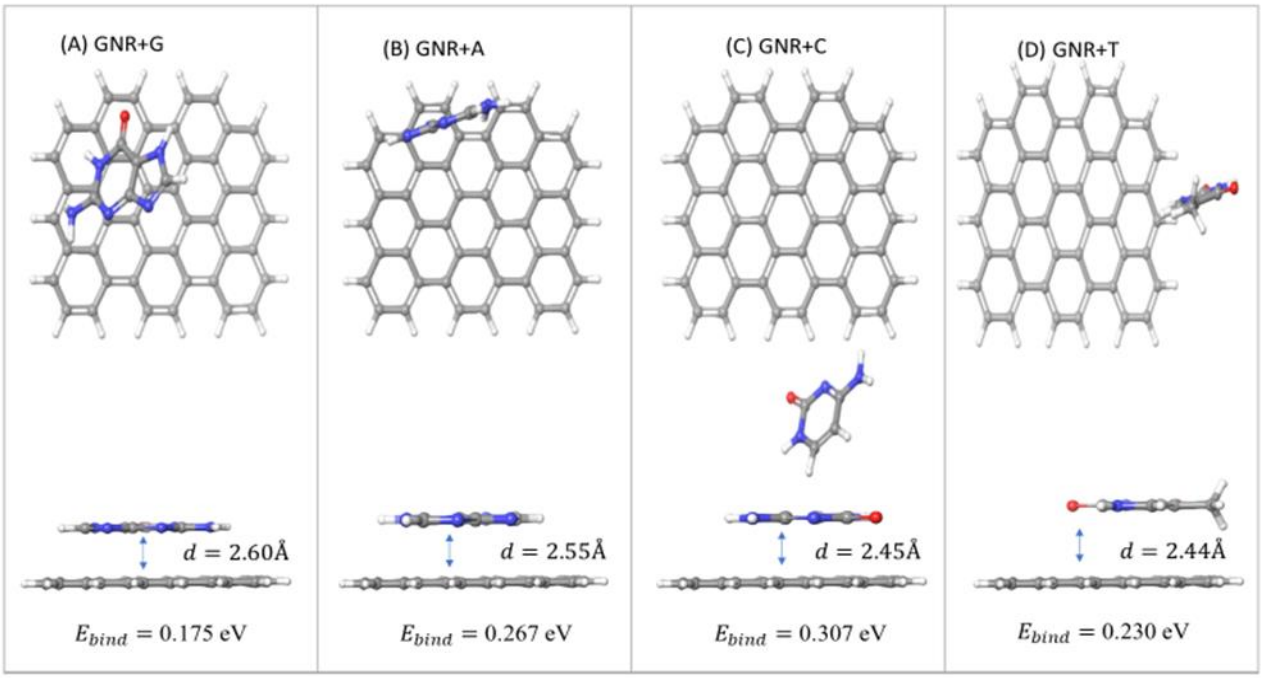

Figure 13: Optimized structures (top and side views) of GNR + bases(grey color represents carbon atom, white for hydrogen, blue for nitrogen and red for oxygen).

Looking at the structures on Figure 13, the equilibrium vertical distance of bases above GNR surface are in the range of 0.244 nm to 0.260 nm. The minimum separation distance was measured to be 0.260 nm for GNR+G, 0.255 nm for GNR+A, 0.245 nm for GNR+C and 0.244 nm for GNR+T. As similar to GNP, the bases seem to be move towards the edges of the GNR.

A plot of the density of states is shown in Figure 14. The changes in density of states going from pristine to combined is more pronounce when compared to the GNP (see Figure 11). This signifies the achieving of better signal in the physisorption process. Also the wider bandgap can be observed.

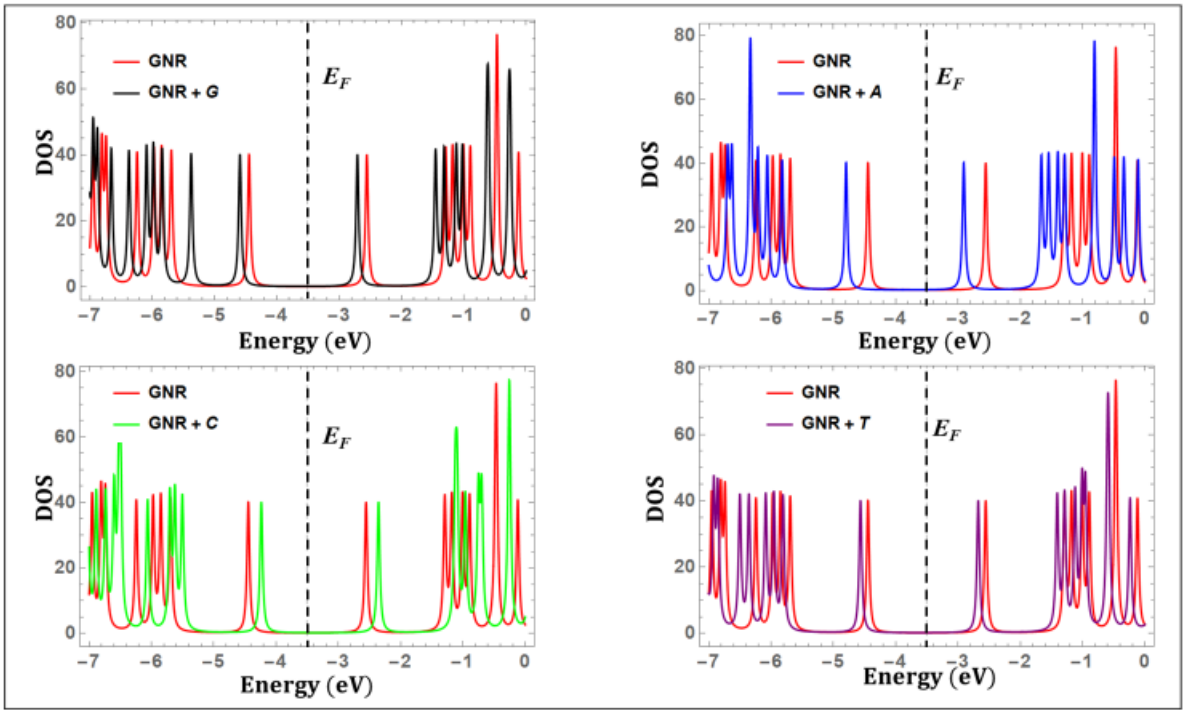

Figure 14: Plot of the density of states for DNA bases and GNR. The dotted lines indicate the positions of Fermi energy level for pristine GNR.

CHAPTER 6

SILICENE

Silicene is a two-dimensional crystal consisting of a single layer of silicon atom. Though there has been lots of speculation about the existence of free standing silicene, the first suggestive structure for silicene was observed in 2010 [53]. A pattern of silicene nanoribbon and silicene sheet deposited on silver crystal were studied using scanning tunneling microscope at atomic resolution. The study shows that silicene has a hexagon honeycomb crystal structure. Silicene is an elemental 2D material consisting of silicon atoms, just as graphene consists of carbon atoms. As silicon and carbon are both group IV elements, their allotropes silicene and graphene possess similar characteristics and properties. Unlike graphene which is flat, silicene has a buckled hexagonal honeycomb structure. This can be due to weak the weak pi bond that arises from the large separation distance between silicon atoms in the hexagonal structure or pseudo-Jahn-Teller effect due to vibronic coupling between closely spaced, filled and empty electronic states [54]. The buckling in silicene provides the tunable bandgap in the presence of an external electric field [55]. A figure of buckled honeycomb structure is shown below.

Figure 15: A single layered buckled honeycomb lattice of Silicene.

The above structure was optimized using DFT simulation. A clear honeycomb lattice can be seen in the Figure 15. The structure of silicene was created using the VESTA software from the CIF of

silicene. The CIF file was obtained from the COD database and extended in two dimensions to get the buckled honeycomb lattice using VESTA. The optimized bond length between silicon atoms in silicene is reported to be 0.2279 nm [56]. Our calculated Si-Si bond length after a geometry optimization calculation was in the range 0.228 nm to 0.236 nm, which agrees nicely with experimental values [59]. The calculated out of plane height was found to be 0.045 nm, which also agrees nicely with the experimental value of 0.044 nm reported by Cahangirov [57]. Unlike graphene which is flat honeycomb lattice with zero bandgap, silicene has a buckled honeycomb lattice structure with direct bandgap. It is therefore important to explore the potential of silicene for DNA sequencing as this material might perform better than graphene. Similar to graphene, we shall focus on two sensing methodologies, that is the silicene nanopore (SNP) and silicene nanoribbon (SNR) devices.

6.1 DNA SENSING USING SILICENE NANOPORE

DNA sequencing using silicene nanopore (SNP) is similar what was already discussed for the graphene nanopore method. The model of the device is shown in Figure 1. A pore of length 13.45 Å and width 11.97 Å was created on the silicene sheet with a total of 160 atoms. Due to the buckled structure of the silicene sheet, creating a symmetrical pore for silicene was not possible. All the edge atoms of the silicene sheet were terminated by adding hydrogen atoms. A geometry optimization calculation was performed for the pristine system B3LYP potential energy model and 6-31G (d,p) basis set. The optimized geometry for the silicene pore is shown in Figure 16.

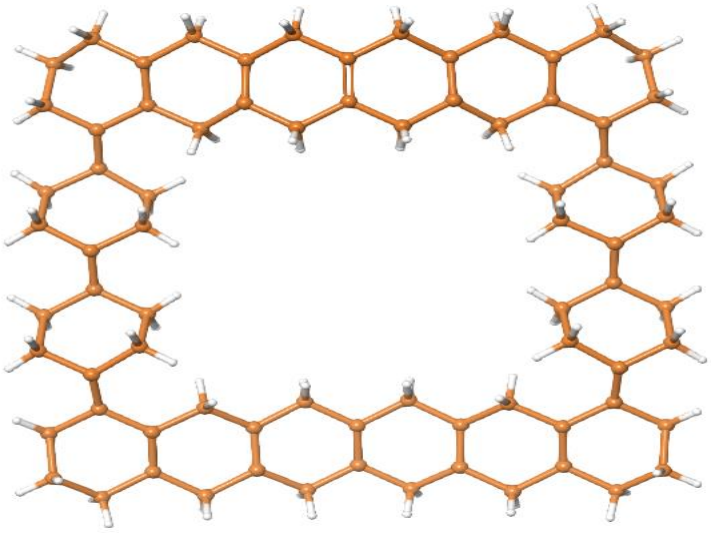

Figure 16: Silicene nanopore created using the Maestro software (orange represents the silicon atom, and white for hydrogen).

The HOMO and LUMO orbital energies were obtained from the output file and the bandgap was calculated for the SNP system. The complete results are summerized in Table 7.

Gaussian output for Silicene nanopore				
2d_elements	Total energy(eV)	Homo(eV)	Lumo(eV)	Bandgap(eV)
Silicene_pore	-600137.492	-5.255	-3.036	2.219

Table 7: A table showing total energy, homo, lumo and bandgap of Silicene nanopore.

To visualize the energy levels of the system, a density of states plot was created using the energies levels from the output file. Figure 17 shows the DOS plot for SNP. The dash line indicates the position of the Fermi energy and a bandgap of 2.219 eV can be seen.

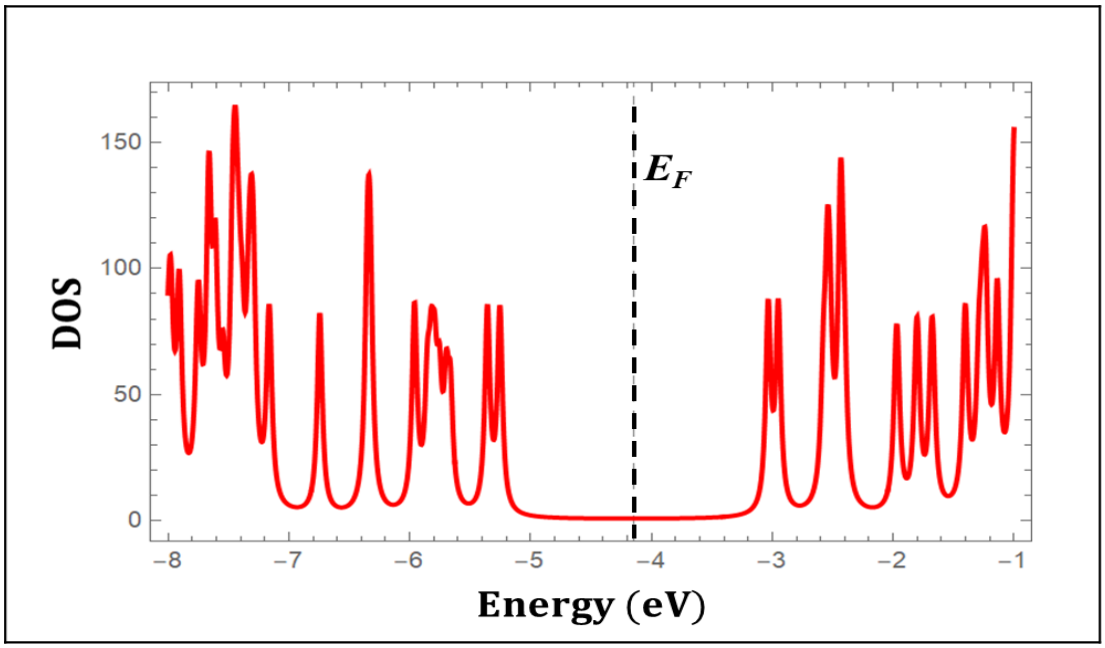

Figure 17: Plot of density of states for pristine SNP showing a bandgap. The dotted line indicates the position of Fermi energy level for pristine SNP.

After the initial calculations for pristine SNP, the next step is to create the structures of SNP+ DNA bases. The molecular editor software Maestro was used to insert the DNA bases inside the pore and create the structures. These structure were exported to the Avogadro software which was then used for generating Gaussian input files. A DFT calculation was then performed for all the structures, that is SNP +A, SNP + C, SNP + G and SNP + T. The results for all the systems are summeraized in the Table 8.

DNA bases inside silicene nano pore [B3LYP 6-31(d,p)]					
combination	Total energy(eV)	Homo(eV)	Lumo(eV)	Bandgap(eV)	Binding energy(eV)
Silicene_adenine	-612854.059	-5.192	-3.124	2.068	-0.213
Silicene_cytosine	-610884.705	-5.167	-3.069	2.098	-0.306
Silicene_guanine	-614901.652	-5.246	-3.102	2.144	-0.234
Silicene_thymine	-612495.739	-5.232	-3.055	2.176	-0.222

Table 8: A table summarizing the output results from the DFT calculation for DNA bases inside the silicene nanopore.

From Table 8, the bandgap ranges from 2.068 eV to 2.176 eV and the binding energy ranges from -0.305 eV to -0.213 eV. The larger the binding energy, the stronger the interaction between the bases and silicene pore. SNP+T has the highest bandgap of 2.176 eV and binding energy of -0.222 eV, SNP+A has the lowest bandgap of 2.068 eV and binding energy of -0.213 eV. To visualize the the relationship between the bandgap and binding energy, a plot was created.

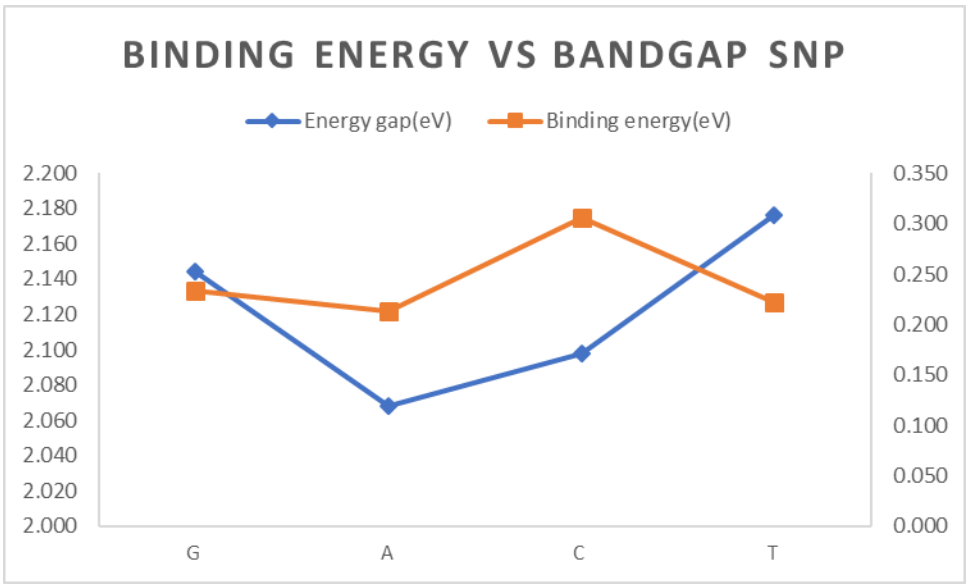

Figure 18: A chart comparing binding energy and bandgap of SNP+DNA bases.

From Figure 18, the energy gap decreases from SNP+G to SNP+A and then increases steadily from SNP + A to SNP + T. In the other hand, the binding energy lacks a clear trend.

The optimized geometry of the SNP with bases is shown in Figure 19.

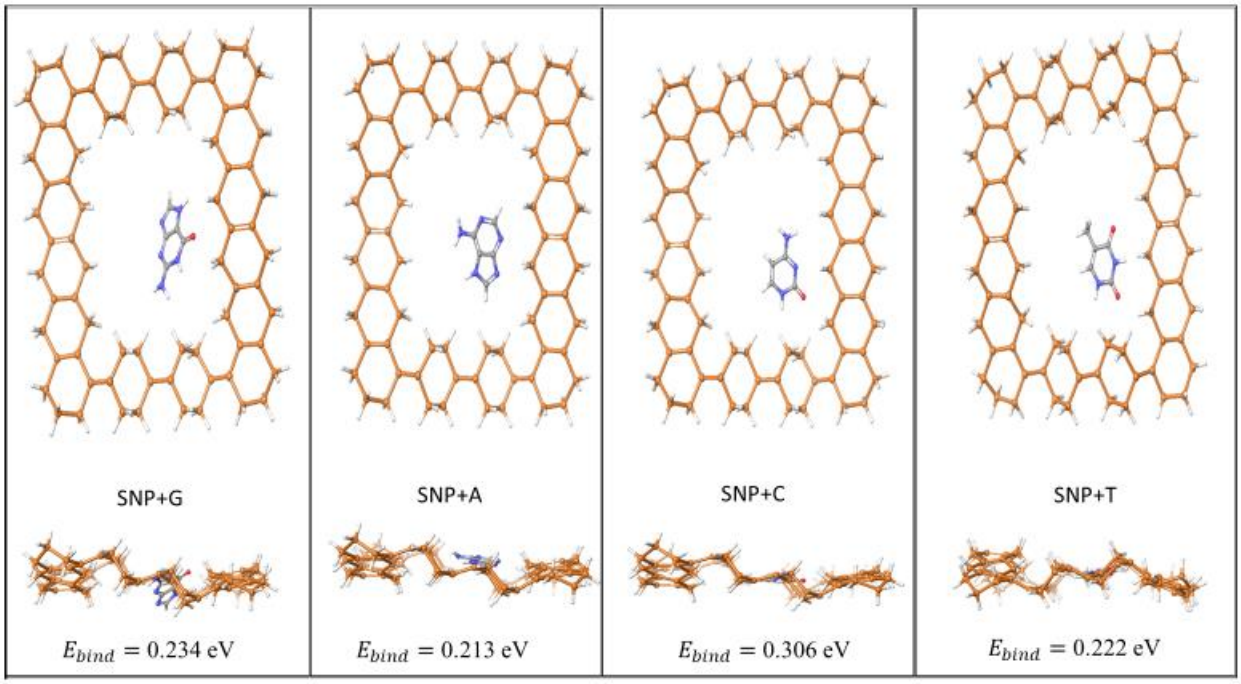

Figure 19: Optimized structures (top and side views) of SNP + BASES (gold color represents silicon atom, white hydrogen, blue nitrogen and red for oxygen).

From Figure 19, we observe less displacement of bases inside pore as compared to graphene. The bases seem to remain approximately in plane with the silicene nanopore surface. Unlike GNP where basis move towards edges of the pore during translocation (see Figure 7), in SNP, the bases stay approximately in place. This indicates that the tendency of bases to stick on the edges of the SNP is minimal. This observation shows that SNP would produce a better read out of DNA bases and can be used for high speed sequencing compared to graphene where bases stick to edges of pore during translocation and slow down speed of translocation and can even cause pore clogging [28]. Next, we analyze the density of states. Figure 20 shows the density of states for the SNP + DNA base systems.

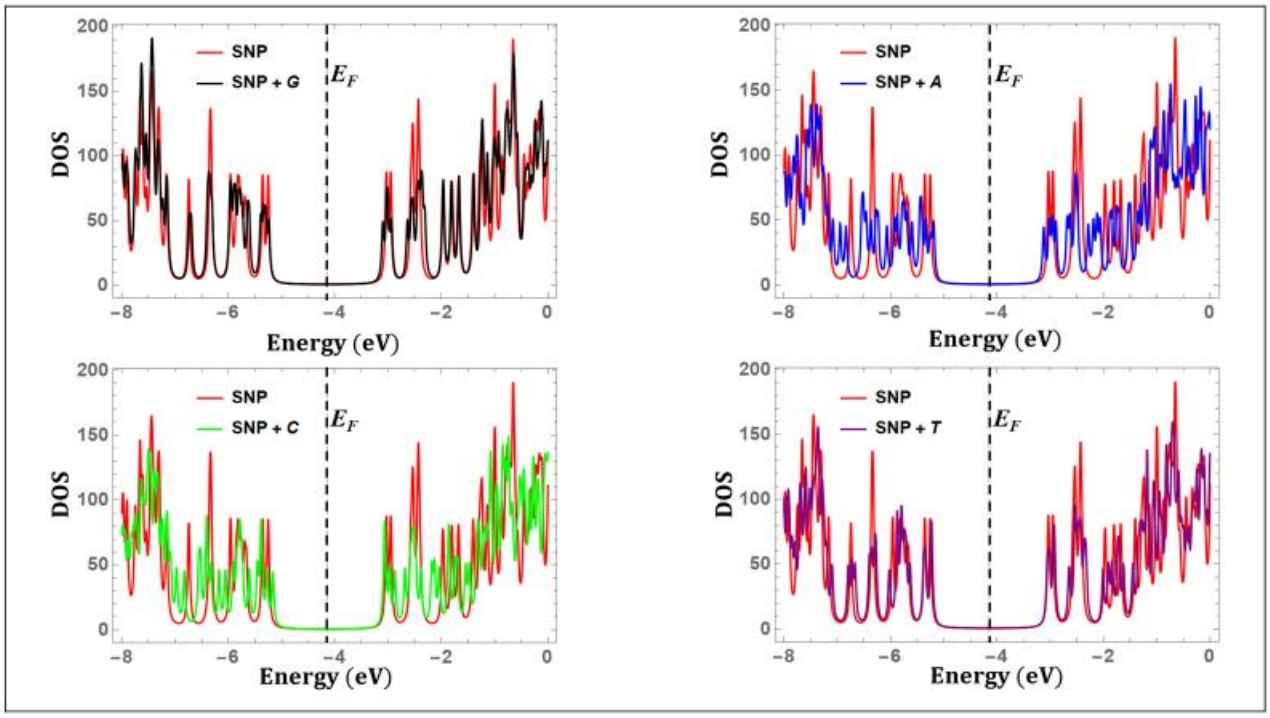

Figure 20: Plot of the density of states for DNA bases + SNP. The dotted lines indicate the positions of the Fermi energy level for pristine SNP.

Looking at Figure 20, we observe that the change in bandgap and DOS is unique for each base. Also, the change in bandgap is large for the SNP device than the GNR device, again confirming the hypothesis that silicene might be a superior sensing material when compared to graphene.

6.2 DNA SENSING USING SILICENE NANORIBBON (PHYSISORPTION)

In this method, we study the modulations in the electronic properties of silicene nanoribbon (SNR) due to physisorption of DNA bases on its surface.

First we created a silicene nanomaterial with width larger than the size of a DNA base. The SNR system has 104 atoms, length of 21.84 Å in long and width of 20.73 Å. The structure is was then optimized using DFT. Figure 21 shows the top and lateral views of the optimized SNR. In the top view, a hexagonal structure can be observed, whereas the lateral view shows the buckled shape.

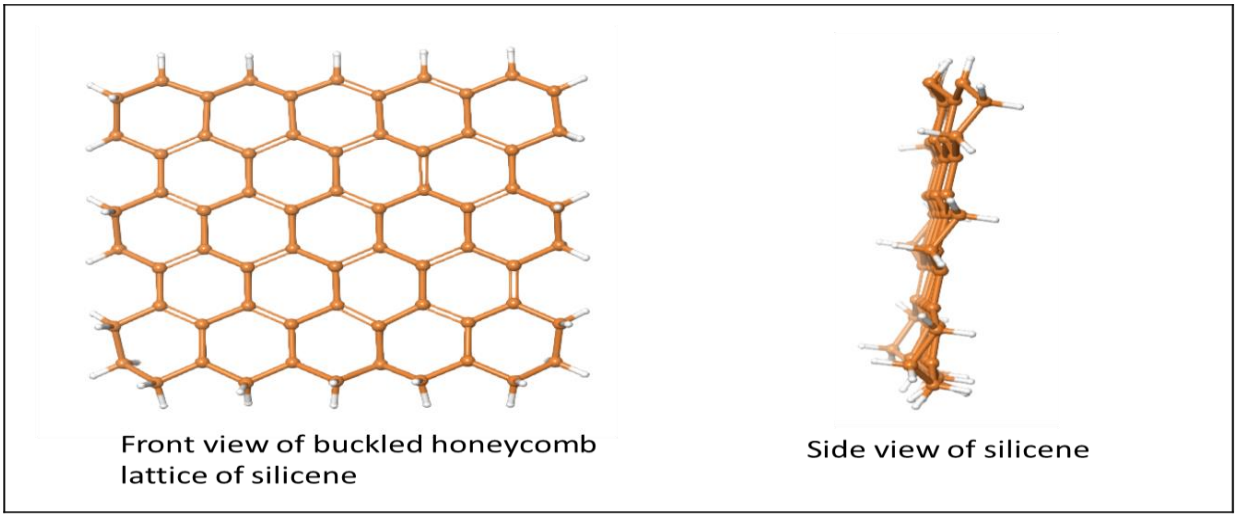

Figure 21: An optimized structure of pristine SNR.

From the DFT calculation for pristine SNR, a HOMO energy of -4.540 eV, LUMO energy of -4.192 eV, and bandgap of 0.348 eV were obtained.

Gaussian output for Silicene nano ribbon (physisorption)				
2d_elements	Total energy(eV)	Homo(eV)	Lumo(eV)	Bandgap(eV)
SNR	-520541.990	-4.540	-4.192	0.348

Table 9: A table showing total energy, HOMO, LUMO and bandgap of pristine SNR.

To visualize the molecular energy levels of the system, we plotted the density of states as shown in Figure 22. From Figure 22, we can notice a small bandgap of 0.348 eV for pristine SNR.

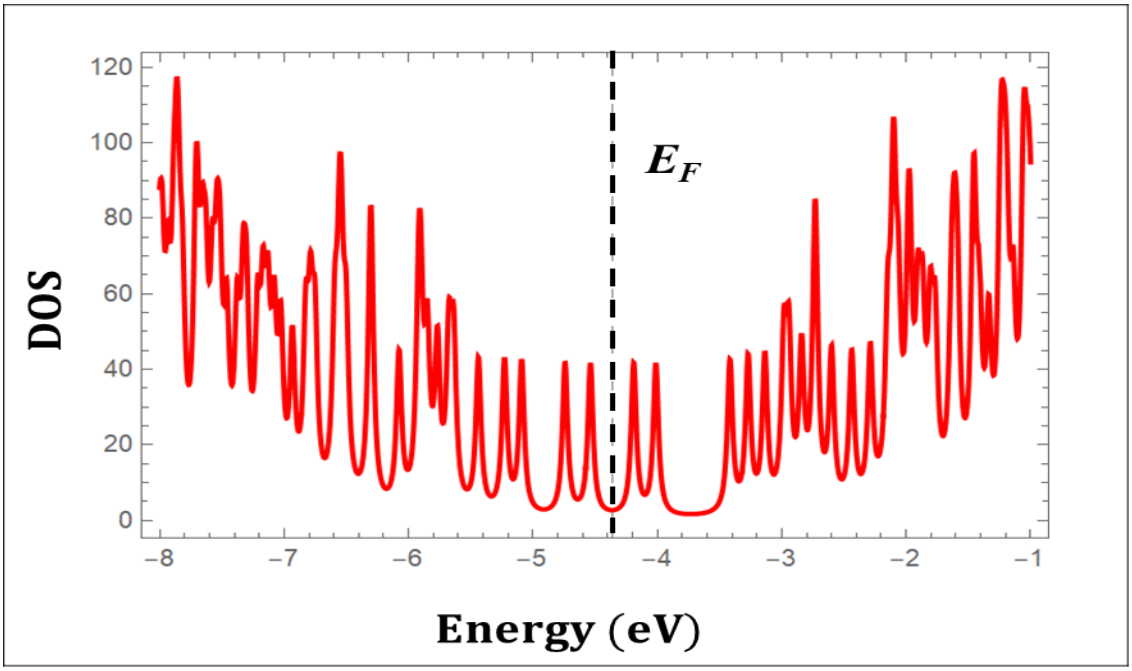

Figure 22: Plot of density of state for pristine Silicene nano ribbon, showing the bandgap. The dotted line indicates the position of Fermi energy level for pristine SNR.

After the initial DFT calculation for pristine SNR, we now turn our attention to SNR + DNA bases systems. DNA bases were kept at a distance of 0.3 nm above center of SNR sheet and DFT calculations were performed for each base. From the outputs, the HOMO and LUMO states were identified and the bandgap and binding energies were calculated as shown in Table 10.

Gaussian output for Physisorption opt geometry B3LYP 6-31(d,p))					
Combination	Total energy(eV)	Homo(eV)	Lumo(eV)	Bandgap(eV)	binding energy(eV)
SNR+G	-535306.409	-4.448	-4.118	0.329	-0.493
SNR+A	-533258.524	-4.553	-4.181	0.372	-0.180
SNR+C	-531289.530	-4.388	-4.022	0.366	-0.633
SNR+T	-532900.109	-4.498	-4.154	0.344	-0.094

Table 10: A table summarizing the output results from the DFT calculation for SNR + DNA bases.

For silicene nanoribbon devices, the energy bandgap for the equilibrium system is in the range of 0.329 eV to 0.372 eV. Whereas the binding energy is in the range of 0.094 eV to 0.633 eV. Figure

23 shows the relationship between binding energy and bandgap for each of the DNA base. The binding energy for SNR+C is the highest among all followed by SNR+G, SNR+A, and SNR+T. On the other hand, the bandgap variation is such that SNR+G >SNR+T >SNR+C >SNR+A.

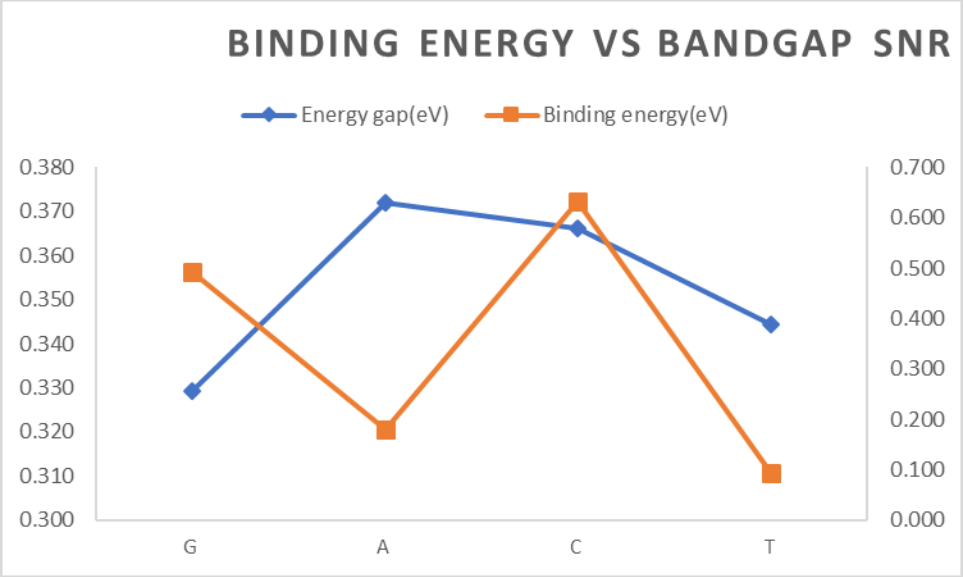

Figure 23: A chart comparing binding energy and bandgap of SNR+DNA bases.

To visualize and analyze the structural changes after the geometry optimization procedure, a figure was created combining all the systems. Figure 24 shows the final structures of all the SNR+base systems.

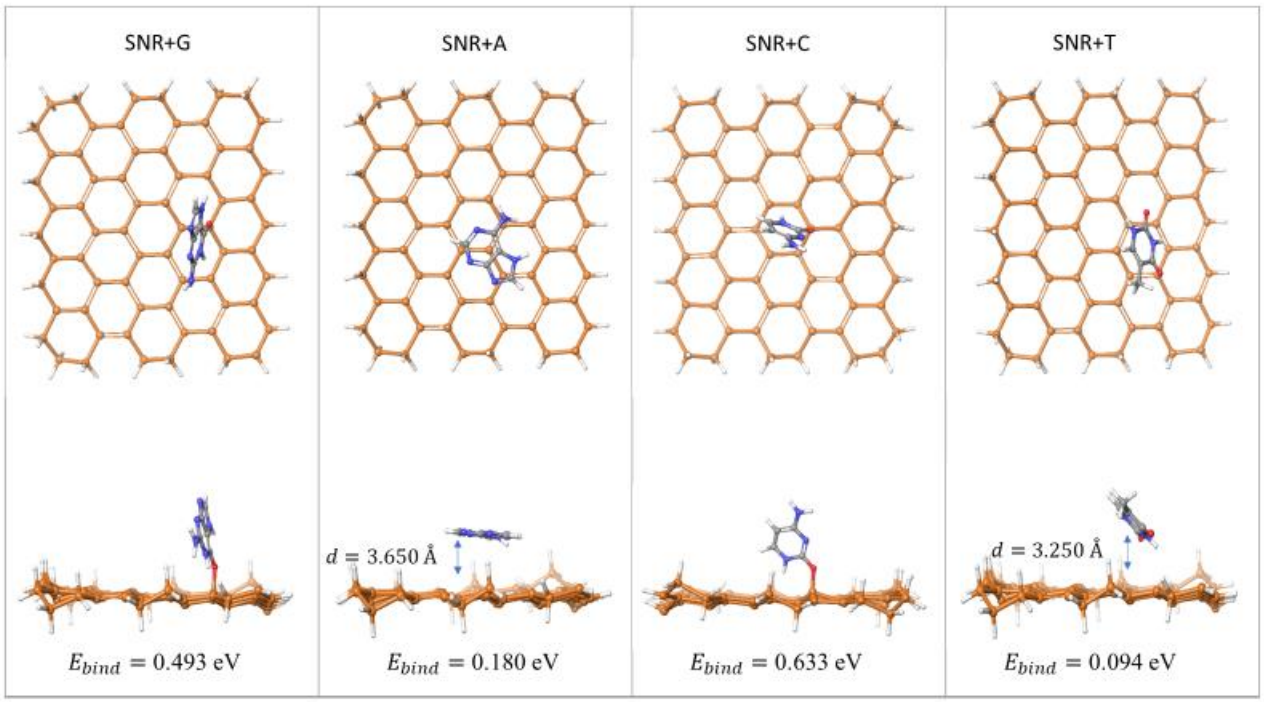

Figure 24: Optimized structures (top and side views) of SNR + BASES.

In the optimized geometry, we noticed that guanine and cytosine each sticks with to surface of the SNR and forms a covalent bond. Unlike gaunine and cytosine, no sticking was observed for adenine and thymine. The optimized vertical distance above surface of the SNR was calculated as 0.365 nm and 0.325 nm for SNR+A and SNR+T, respectively.

To visualize the distribution of energy states, the density of states plot was created, as shown in Figure 25. From Figure 25, we observe small modulations in the DOS for the pristine SNR. The change is DOS for SNR seems to be smaller compared to the SNP device (see Figure 20). The differnce in density of state of pristine SNR to SNR+bases is less distinct, so we can conclude SNP to give more better current as compare to SNR. The bandgap for SNR in the presence of the DNA bases was comparable to those for the SNP system.

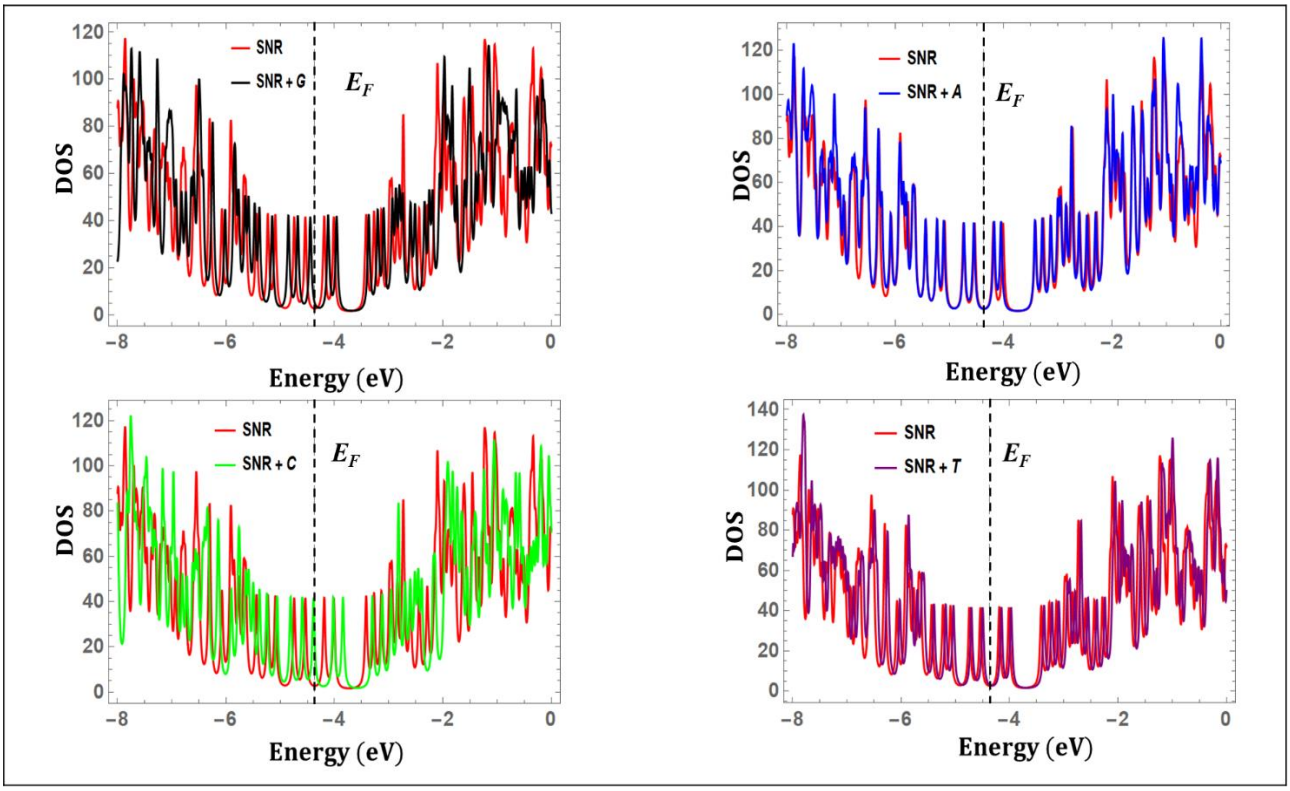

Figure 25: Plot of the density of states for DNA bases with SNR. The dotted lines indicate the positions of fermi energy level for pristine SNP.

CHAPTER 7

RESULTS AND CONCLUSION

In summary, DFT calculations were performed to evaluate the potential of silicene as a candidate material for DNA sequencing using two detection principles, namely the nanopore and nanoribbon devices. As graphene is the mostly widely studied 2D material for DNA sequencing, we benchmarked our results by comparing with graphene. Starting with nanopore method, we observed that the magnitude of binding energies for graphene devices were higher than those for the silicene devices. This signifies stronger interaction that can cause more electrons to tunnel through nanopore, hence given rise to a better signal.

For graphene nanopore, the binding energy varies as GNP+G > GNP+C > GNP+A > GNP+T, while for silicene, it varies as SNP+C > SNP+G >SNP+T > SNP+A. Figure 26 is a bar plot that shows the binding energy comparison for graphene and silicene nanopores for each DNA base.

Binding Energy (eV)		
	GNP	SNP
Guanine	0.430	0.234
Adenine	0.361	0.213
Cytosine	0.418	0.306
Thymine	0.282	0.222

Table 11: Comparison of binding energy for graphene nanopore and silicene nanopore with DNA bases.

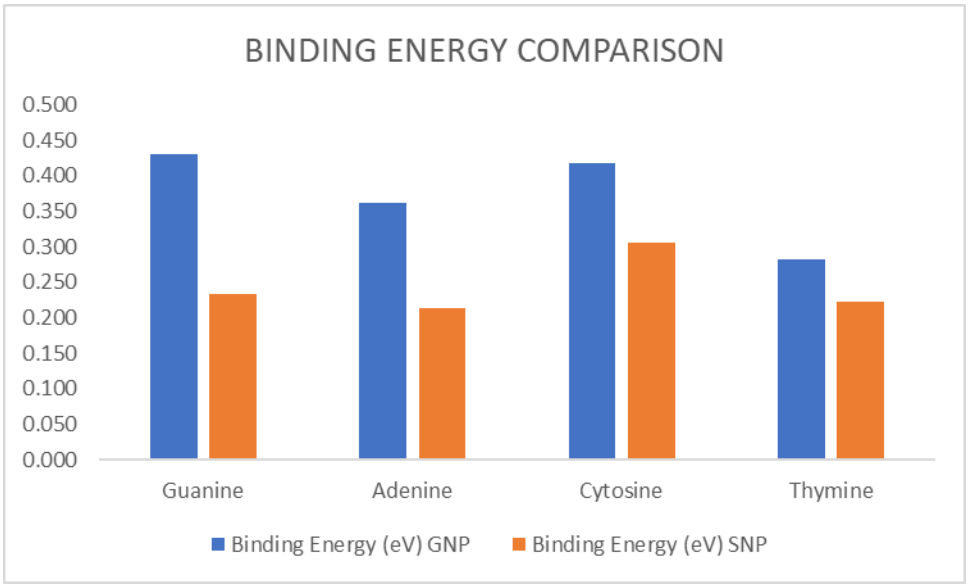

Figure 26: Bar graph comparing the binding energies for graphene and silicene nanopores for different bases.

From Figure 26, we observe that the binding energies for GNP is greater than those for SNP It was also observed that the displacement of bases in the nanopore (from initial central position before optimization) was greater for GNP compared to SNP.

Another important property of interest is the bandgap. Table 12 shows the bandgap for GNP and SNP systems. The bandgaps obtained are higher in magnitude in SNP compared to GNP.

Band Gap (eV)		
	GNP	SNP
Pristine	1.048	2.219
Guanine	1.067	2.144
Adenine	1.031	2.068
Cytosine	1.088	2.098
Thymine	1.049	2.176

Table 12: Comparison of bandgap for GNP and SNP with bases.

To further investigate and quantify the interaction between GNP (and SNP) with bases, we calculated the change in bandgap (ΔEgap) as;

$$\Delta E_{gap} = E_{gap}^{nanopore+bases} - E_{gap}^{nanopore} \quad (6)$$

where $E_{gap}^{nanopore+bases}$ is the bandgap of the combined system, that is GNP+bases (or SNP+bases), and $E_{gap}^{nanopore}$ is the bandgap of the pristine system. In our calculations, only the absolute value of the difference is reported, as we are only trying to compare the magnitude of the change. On Table 13, we see that the change in bandgap is generally larger for SNP compared to GNP. For SNP, the change in bandgap varies as of SNP+A > SNP+C > SNP+G > SNP+T, whereas for GNP, the sequence is GNP+C > GNP+G > GNP+A > GNP+T. Based on this result, one can conclude that silicene nanopore is more likely to produce a more distinguishable signal compared to graphene nanopore.

Enery gap (ΔE) (eV)		
	GNP	SNP
Guanine	0.019	0.074
Adenine	0.017	0.150
Cytosine	0.039	0.121
Thymine	0.001	0.042

Table 13: Energy gap comparison for GNP and SNP with bases.

The other detection method studied is the nanoribbon (physisorption) technique. Table 14 and Table 15 shows the complete results for binding energy and bandgap for physisorption of graphene and silicene with bases. For graphene, it is seen that the GNR has a larger bandgap and relatively lower binding energy as compared to the GNP. Whereas, SNR has a lower bandgap, but similar

range of binding energy as compared to SNP. We also observe from Table 14 that the binding energy is stronger in GNR (for adenine and thymine) compared to SNR. For cytosine and guanine, the binding energy in GNR is less compared to SNR.

Binding Energy (eV)		
	GNR	SNR
Guanine	0.175	0.493
Adenine	0.267	0.180
Cytosine	0.307	0.633
Thymine	0.230	0.094

Table 14: Binding comparison between GNR and SNR with bases.

Band Gap (eV)		
	GNR	SNR
Pristine	1.891	0.348
Guanine	1.885	0.329
Adenine	1.889	0.372
Cytosine	1.882	0.366
Thymine	1.890	0.344

Table 15: Bandgap comparison between GNR and SNR with bases.

Another useful property of interest for physisorption is the minimum equilibrium vertical distance between bases and nanoribbon surface. Table 16 shows the minimum vertical distance for GNR and SNR. In the optimized geometry, we noticed that guanine and cytosine each sticks to the surface of the SNR and forms a covalent bond. Unlike gaunine and cytosine, no sticking was observed for adenine and thymine. The optimized vertical distance above surface of the SNR was calculated as 0.365 nm and 0.325 nm for SNR+A and SNR+T, respectively. No sticking was observed for GNR.

This property is related to the binding energy, since binding energy is inversely proportional to distance.

Vertical distance in Å		
	SNR	GNR
Guanine	-	2.600
Adenine	3.650	2.550
Cytosine	-	2.450
Thymine	3.250	2.440

Table 16: Optimized minimum vertical distance of GNR and SNR with bases.

Finally, we compare the change in energy gap for SNR and GNR, as shown in Table 17. In case of physisorption, with the available data, SNR seems to have better energy gap value to the GNR.

Enery gap (ΔE) (eV)		
	GNR	SNR
Guanine	0.005	0.019
Adenine	0.002	-0.024
Cytosine	0.009	-0.019
Thymine	0.001	0.004

Table 17: Energy gap comparison on GNR and SNR with bases.

Considering all the results analyzed in this thesis, one could conclude that SNP is likely to produce stronger and distinguishable current signals for each DNA base when used in real devices, compared to GNP. The sticking of bases on the surface of the SNR device makes it less suitable for use in practical applications. Future directions would involve extending these calculations to periodic systems and studying device properties such as current-voltage characteristics using the non-equilibrium Green's function technique. We hope that the findings from this research has shed useful insights that can guide further experimental research and development in the field of DNA sequencing using 2D materials.

REFERENCES

[1] S. J. Heerema and C. Dekker, "Graphene nanodevices for DNA sequencing," *Nature Nanotechnology*, vol. 11, no. 2. Nature Publishing Group, pp. 127–136, Feb. 01, 2016, doi: 10.1038/nnano.2015.307.

[2] R. Varnai *et al.*, "Pharmacogenomic biomarker information differences between drug labels in the United States and Hungary: implementation from medical practitioner view," *Pharmacogenomics J.*, vol. 20, no. 3, pp. 380–387, Jun. 2020, doi: 10.1038/s41397-019-0123-z.

[3] J. J. Kasianowicz, E. Brandin, D. Branton, and D. W. Deamer, "Characterization of individual polynucleotide molecules using a membrane channel," in *Proceedings of the National Academy of Sciences of the United States of America*, Nov. 1996, vol. 93, no. 24, pp. 13770–13773, doi: 10.1073/pnas.93.24.13770.

[4] C. Dekker, "Solid-state nanopores," *Nature Nanotechnology*, vol. 2, no. 4. Nature Publishing Group, pp. 209–215, 2007, doi: 10.1038/nnano.2007.27.

[5] C. Plesa, S. W. Kowalczyk, R. Zinsmeester, A. Y. Grosberg, Y. Rabin, and C. Dekker, "Fast translocation of proteins through solid state nanopores," *Nano Lett.*, vol. 13, no. 2, pp. 658–663, Feb. 2013, doi: 10.1021/nl3042678.

[6] D. S. Talaga and J. Li, "Single-molecule protein unfolding in solid state nanopores," *J. Am. Chem. Soc.*, vol. 131, no. 26, pp. 9287–9297, Jul. 2009, doi: 10.1021/ja901088b.

[7] J. Li, D. Stein, C. McMullan, D. Branton, M. J. Aziz, and J. A. Golovchenko, "Ion-beam sculpting at nanometre length scales," *Nature*, vol. 412, no. 6843, pp. 166–169, Jul. 2001, doi: 10.1038/35084037.

[8] J. Feng *et al.*, "Identification of single nucleotides in MoS 2 nanopores," *Nat. Nanotechnol.*, vol. 10, no. 12, pp. 1070–1076, Dec. 2015, doi: 10.1038/nnano.2015.219.

[9] H. Kwok, K. Briggs, and V. Tabard-Cossa, "Nanopore Fabrication by Controlled Dielectric Breakdown," *PLoS One*, vol. 9, no. 3, p. e92880, Mar. 2014, doi: 10.1371/journal.pone.0092880.

[10] M. Van Den Hout, A. R. Hall, M. Y. Wu, H. W. Zandbergen, C. Dekker, and N. H. Dekker, "Controlling nanopore size, shape and stability," *Nanotechnology*, vol. 21, no. 11, p. 115304, Feb. 2010, doi: 10.1088/0957-4484/21/11/115304.

[11] T. Gilboa, A. Zrehen, A. Girsault, and A. Meller, "Optically-Monitored Nanopore Fabrication Using a Focused Laser Beam," *Sci. Rep.*, vol. 8, no. 1, pp. 1–10, 2018, doi: 10.1038/s41598-018-28136-z.

[12] Y. Yuan *et al.*, "Sub-20 nm Nanopores Sculptured by a Single Nanosecond Laser Pulse," *arXiv*, Jun. 2018, Accessed: Nov. 18, 2020. [Online]. Available: http://arxiv.org/abs/1806.08172.

[13] A. J. Storm, J. H. Chen, X. S. Ling, H. W. Zandbergen, and C. Dekker, "Fabrication of solid-state nanopores with single-nanometre precision," *Nature Materials*, vol. 2, no. 8. European Association for Cardio-Thoracic Surgery, pp. 537–540, 2003, doi:

10.1038/nmat941.

[14] B. M. Venkatesan, A. B. Shah, J. M. Zuo, and R. Bashir, “DNA sensing using nanocrystalline surface-enhanced Al2O 3 nanopore sensors,” *Adv. Funct. Mater.*, vol. 20, no. 8, pp. 1266–1275, Apr. 2010, doi: 10.1002/adfm.200902128.

[15] A. Mara, Z. Siwy, C. Trautmann, J. Wan, and F. Kamme, “An asymmetric polymer nanopore for single molecule detection,” *Nano Lett.*, vol. 4, no. 3, pp. 497–501, Mar. 2004, doi: 10.1021/nl035141o.

[16] A. Meller, L. Nivon, E. Brandin, J. Golovchenko, and D. Branton, “Rapid nanopore discrimination between single polynucleotide molecules,” *Proc. Natl. Acad. Sci. U. S. A.*, vol. 97, no. 3, pp. 1079–1084, Feb. 2000, doi: 10.1073/pnas.97.3.1079.

[17] G. M. Skinner, M. Van Den Hout, O. Broekmans, C. Dekker, and N. H. Dekker, “Distinguishing single-and double-stranded nucleic acid molecules using solid-state nanopores,” *Nano Lett.*, vol. 9, no. 8, pp. 2953–2960, Aug. 2009, doi: 10.1021/nl901370w.

[18] A. J. Storm, J. H. Chen, H. W. Zandbergen, and C. Dekker, “Translocation of double-strand DNA through a silicon oxide nanopore,” *Phys. Rev. E - Stat. Nonlinear, Soft Matter Phys.*, vol. 71, no. 5, p. 051903, May 2005, doi: 10.1103/PhysRevE.71.051903.

[19] M. Graf *et al.*, “Fabrication and practical applications of molybdenum disulfide nanopores,” *Nat. Protoc.*, vol. 14, no. 4, pp. 1130–1168, 2019, doi: 10.1038/s41596-019-0131-0.

[20] W. Si and A. Aksimentiev, “Nanopore Sensing of Protein Folding,” *ACS Nano*, vol. 11, no. 7, pp. 7091–7100, Jul. 2017, doi: 10.1021/acsnano.7b02718.

[21] D. Branton *et al.*, “The potential and challenges of nanopore sequencing,” *Nat. Biotechnol.*, vol. 26, no. 10, pp. 1146–1153, 2008, doi: 10.1038/nbt.1495.

[22] E. C. Yusko *et al.*, “Real-time shape approximation and fingerprinting of single proteins using a nanopore,” *Nat. Nanotechnol.*, vol. 12, no. 4, pp. 360–367, May 2017, doi: 10.1038/nnano.2016.267.

[23] M. Drndić, “Sequencing with graphene pores,” *Nat. Nanotechnol.*, vol. 9, no. 10, p. 743, 2014, doi: 10.1038/nnano.2014.232.

[24] J. K. Rosenstein, M. Wanunu, C. A. Merchant, M. Drndic, and K. L. Shepard, “Integrated nanopore sensing platform with sub-microsecond temporal resolution,” *Nat. Methods*, vol. 9, no. 5, pp. 487–492, May 2012, doi: 10.1038/nmeth.1932.

[25] K. S. Novoselov, A. Mishchenko, A. Carvalho, and A. H. Castro Neto, “2D materials and van der Waals heterostructures,” *Science*, vol. 353, no. 6298. American Association for the Advancement of Science, Jul. 29, 2016, doi: 10.1126/science.aac9439.

[26] S. Z. Butler *et al.*, “Progress, challenges, and opportunities in two-dimensional materials beyond graphene,” *ACS Nano*, vol. 7, no. 4. American Chemical Society, pp. 2898–2926, Apr. 23, 2013, doi: 10.1021/nn400280c.

[27] A. K. Geim and I. V Grigorieva, “Van der Waals heterostructures,” *Nature*, vol. 499, no. 7459, pp. 419–425, 2013, doi: 10.1038/nature12385.

[28] T. Nelson, B. Zhang, and O. V. Prezhdo, “Detection of nucleic acids with graphene nanopores: Ab initio characterization of a novel sequencing device,” *Nano Lett.*, vol. 10, no. 9, pp. 3237–3242, Sep. 2010, doi: 10.1021/nl9035934.

[29] S. Garaj, W. Hubbard, A. Reina, J. Kong, D. Branton, and J. A. Golovchenko, “Graphene as a subnanometre trans-electrode membrane,” *Nature*, vol. 467, no. 7312, pp. 190–193, Sep. 2010, doi: 10.1038/nature09379.

[30] C. A. Merchant *et al.*, “DNA translocation through graphene nanopores,” *Nano Lett.*, vol. 10, no. 8, pp. 2915–2921, Aug. 2010, doi: 10.1021/nl101046t.

[31] D. B. Wells, M. Belkin, J. Comer, and A. Aksimentiev, “Assessing graphene nanopores for sequencing DNA,” *Nano Lett.*, vol. 12, no. 8, pp. 4117–4123, Aug. 2012, doi: 10.1021/nl301655d.

[32] C. Sathe, X. Zou, J. P. Leburton, and K. Schulten, “Computational investigation of DNA detection using graphene nanopores,” *ACS Nano*, vol. 5, no. 11, pp. 8842–8851, Nov. 2011, doi: 10.1021/nn202989w.

[33] A. B. Farimani, K. Min, and N. R. Aluru, “DNA base detection using a single-layer MoS2,” *ACS Nano*, vol. 8, no. 8, pp. 7914–7922, 2014, doi: 10.1021/nn5029295.

[34] G. F. Schneider *et al.*, “Tailoring the hydrophobicity of graphene for its use as nanopores for DNA translocation,” *Nat. Commun.*, vol. 4, no. 1, pp. 1–7, Oct. 2013, doi: 10.1038/ncomms3619.

[35] W. Lv *et al.*, “Interlayer Water Regulates the Bio-nano Interface of a β-sheet Protein stacking on Graphene,” *Sci. Rep.*, vol. 5, no. 1, p. 7572, 2015, doi: 10.1038/srep07572.

[36] L. Zhang and X. Wang, “DNA Sequencing by Hexagonal Boron Nitride Nanopore: A Computational Study,” *Nanomaterials*, vol. 6, no. 6, p. 111, Jun. 2016, doi: 10.3390/nano6060111.

[37] S. Liu *et al.*, “Boron nitride nanopores: Highly sensitive DNA single-molecule detectors,” *Adv. Mater.*, vol. 25, no. 33, pp. 4549–4554, Sep. 2013, doi: 10.1002/adma.201301336.

[38] J. Li, D. Fologea, R. Rollings, and B. Ledden, “Characterization of Protein Unfolding with Solid-state Nanopores,” *Protein Pept. Lett.*, vol. 21, no. 3, pp. 256–265, Jan. 2014, doi: 10.2174/09298665113209990077.

[39] J. Li *et al.*, “Molecular dynamics study of DNA translocation through graphene nanopores,” *Phys. Rev. E - Stat. Nonlinear, Soft Matter Phys.*, vol. 87, no. 6, p. 062707, Jun. 2013, doi: 10.1103/PhysRevE.87.062707.

[40] M. Sun, Q. Ren, S. Wang, J. Yu, and W. Tang, “Electronic properties of Janus silicene: New direct band gap semiconductors,” *J. Phys. D. Appl. Phys.*, vol. 49, no. 44, p. 445305, Oct. 2016, doi: 10.1088/0022-3727/49/44/445305.

[41] M. Tsutsui, M. Taniguchi, K. Yokota, and T. Kawai, “Identifying single nucleotides by

tunnelling current," *Nat. Nanotechnol.*, vol. 5, no. 4, pp. 286–290, Apr. 2010, doi: 10.1038/nnano.2010.42.

[42] M. Tsutsui, M. Taniguchi, and T. Kawai, "Transverse field effects on DNA-sized particle dynamicsn," *Nano Lett.*, vol. 9, no. 4, pp. 1659–1662, Apr. 2009, doi: 10.1021/nl900177q.

[43] Y. Wang, Q. Yang, Z. Wang, and G. Lab, "The evolution of nanopore sequencing," 2015, doi: 10.3389/fgene.2014.00449.

[44] K. H. Paik *et al.*, "Control of DNA capture by nanofluidic transistors," *ACS Nano*, vol. 6, no. 8, pp. 6767–6775, Aug. 2012, doi: 10.1021/nn3014917.

[45] J. Lee, Y. Choi, H. Kim, R. H. Scheicher, and J. Cho, "Physisorption of DNA Nucleobases on h - BN and Graphene : vdW- Corrected DFT Calculations," 2013, doi: 10.1021/jp402403f.

[46] "DNA: Definition, Structure & Discovery | What Is DNA? | Live Science." https://www.livescience.com/37247-dna.html (accessed Sep. 03, 2020).

[47] G. Ferry, "The structure of DNA," *Nature*, vol. 575, no. 7781. NLM (Medline), pp. 35–36, Nov. 01, 2019, doi: 10.1038/d41586-019-02554-z.

[48] P. C. W. Davies, "Quantum tunneling time," *Am. J. Phys.*, vol. 73, no. 1, pp. 23–27, Jan. 2005, doi: 10.1119/1.1810153.

[49] R. G. Amorim and R. H. Scheicher, "Silicene as a new potential DNA sequencing device," 2015, doi: 10.1088/0957-4484/26/15/154002.

[50] T. M. McCormick *et al.*, "Conjugated polymers: Evaluating DFT methods for more accurate orbital energy modeling," *Macromolecules*, vol. 46, no. 10, pp. 3879–3886, May 2013, doi: 10.1021/ma4005023.

[51] "Metals, Semiconductors, and Insulators."

[52] Z. Zhen and H. Zhu, *Structure and properties of graphene*. Elsevier Inc., 2017.

[53] B. Aufray *et al.*, "Graphene-like silicon nanoribbons on Ag(110): A possible formation of silicene," *Appl. Phys. Lett.*, vol. 96, no. 18, p. 3, Jan. 2010, doi: 10.1063/1.3419932.

[54] L. C. Lew Yan Voon, "Electronic structure of silicene," *Chinese Physics B*, vol. 24, no. 8. Institute of Physics Publishing, Aug. 01, 2015, doi: 10.1088/1674-1056/24/8/087309.

[55] D. Jose and A. Datta, "Structures and chemical properties of silicene: Unlike graphene," *Acc. Chem. Res.*, vol. 47, no. 2, pp. 593–602, Feb. 2014, doi: 10.1021/ar400180e.

[56] Z. Ni *et al.*, "Tunable Band Gap and Doping Type in Silicene by Surface Adsorption: towards Tunneling Transistors."

[57] S. Cahangirov, M. Topsakal, E. Aktürk, H. Šahin, and S. Ciraci, "Two- and one-dimensional honeycomb structures of silicon and germanium," *Phys. Rev. Lett.*, vol. 102, no. 23, p. 236804, Jun. 2009, doi: 10.1103/PhysRevLett.102.236804.

Appendix A: Sample Input Files(silcene nanoribbon 104 atoms[silicene.com])

#n B3LYP/6-31G(d,p) Opt

Title

0 1

Si	-11.16170	7.82440	-0.02520
Si	-11.17120	3.83070	-0.20890
Si	-7.83840	5.83520	0.06240
Si	-4.47510	7.78600	0.24630
Si	-11.31270	0.00040	0.47080
Si	-7.84980	1.87970	0.10080
Si	-4.49250	3.86590	0.12750
Si	-1.13070	5.83360	0.18160
Si	2.24440	7.78070	0.17240
Si	-11.17140	-3.82970	-0.20970
Si	-7.84990	-1.87900	0.10060
Si	-4.47290	0.00020	0.18420
Si	-1.12050	1.94400	0.22250
Si	2.23580	3.89680	0.23690
Si	5.61250	5.83280	0.19120
Si	-11.16240	-7.82360	-0.02590
Si	-7.83890	-5.83470	0.06180
Si	-4.49290	-3.86560	0.12720
Si	-1.12070	-1.94390	0.22250
Si	2.24070	-0.00020	0.27470
Si	5.59850	1.97780	0.31030
Si	-11.14870	-11.53210	1.11350
Si	-7.80380	-9.76980	0.31570

Si	-4.47580	-7.78580	0.24590
Si	-1.13130	-5.83360	0.18150
Si	2.23530	-3.89690	0.23710
Si	5.59830	-1.97850	0.31080
Si	-4.39580	-11.69410	0.72560
Si	-1.09690	-9.74880	0.16510
Si	2.24370	-7.78090	0.17270
Si	5.61190	-5.83310	0.19200
Si	2.30410	-11.71890	0.29590
Si	5.61170	-9.74940	-0.11920
Si	-12.35590	5.84790	-0.43620
Si	-8.95000	7.83730	-0.13820
Si	-12.31250	1.81890	-0.67340
Si	-8.95400	3.86020	-0.28700
Si	-5.59850	5.84850	-0.19670
Si	-2.24400	7.79920	-0.15660
Si	-12.31250	-1.81770	-0.67390
Si	-9.11650	0.00040	-0.24950
Si	-5.61760	1.91560	-0.28790
Si	-2.25180	3.88040	-0.23300
Si	1.10720	5.83660	-0.20560
Si	4.47710	7.76750	-0.24700
Si	-12.35620	-5.84690	-0.43690
Si	-8.95420	-3.85940	-0.28730
Si	-5.61770	-1.91510	-0.28820
Si	-2.23320	0.00010	-0.21180
Si	1.12220	1.94250	-0.16420
Si	4.46020	3.89280	-0.18720
Si	-12.35610	-9.84840	-0.01090

Si	-8.95070	-7.83670	-0.13870
Si	-5.59890	-5.84810	-0.19700
Si	-2.25210	-3.88030	-0.23310
Si	1.12200	-1.94260	-0.16430
Si	4.50270	-0.00030	-0.02990
Si	-9.00890	-11.78370	0.15810
Si	-5.60170	-9.77070	0.10230
Si	-2.24470	-7.79910	-0.15680
Si	1.10670	-5.83680	-0.20530
Si	4.45980	-3.89320	-0.18680
Si	-2.28380	-11.72280	-0.31910
Si	1.10780	-9.73690	-0.14180
Si	4.47660	-7.76790	-0.24620
Si	4.41200	-11.66960	-0.75660
H	-11.89410	-12.82100	1.03720
H	-11.01210	-11.15620	2.54700
H	-5.18600	-12.89420	0.33270
H	-4.21300	-11.72420	2.20330
H	1.50580	-12.87500	-0.19950
H	2.49330	-11.88620	1.76390
H	-9.16100	-12.19110	-1.26690
H	-8.23760	-12.84660	0.85950
H	-2.47730	-11.87580	-1.78810
H	-1.49600	-12.88980	0.16660
H	4.21130	-11.69720	-2.23250
H	5.19490	-12.87810	-0.37550
H	-12.91790	5.91770	-1.81780
H	-13.52180	5.82320	0.49320
H	-12.48260	1.74470	-2.15950

H	-13.68810	2.04360	-0.13490
H	-12.48230	-1.74340	-2.16000
H	-13.68820	-2.04260	-0.13570
H	-12.91810	-5.91650	-1.81860
H	-13.52220	-5.82200	0.49240
H	-12.65000	-10.28220	-1.40660
H	-13.66220	-9.59410	0.65990
H	-11.47150	8.23240	0.94820
H	-11.55660	8.62100	-0.67290
H	-4.65560	8.07780	1.29140
H	-4.94720	8.61210	-0.30570
H	2.07310	8.10410	1.20970
H	1.77340	8.59260	-0.40110
H	-8.55560	8.54420	0.60660
H	-8.64010	8.32910	-1.07200
H	-1.77220	8.59070	0.44420
H	-2.06380	8.14520	-1.18510
H	4.65170	7.97450	-1.31320
H	6.51160	5.78360	-0.44060
H	6.50820	1.92090	-0.30550
H	6.50720	-2.00620	-0.30820
H	6.51140	-5.85550	-0.44070
H	6.49400	-9.70980	-0.77500

Appendix B: Sample Batch Script [silicene.sh]

```
#!/bin/bash
#SBATCH --job-name=g16
#SBATCH --nodes=2
#SBATCH --cpus-per-task=20
#SBATCH --output=g16-%j.out
#SBATCH --partition=general

### Of the batch options, it is only recommnded to change "--job-name", "--nodes", and
### "--output". Any other modifications may result in an error.

### It is only recommneded to change the input file in the Gaussian command. If needed
### more g16 options can be added.

#Load Gaussian module
module load Gaussian/g16

#Gaussian scratch directory.
export GAUSS_SCRDIR=/home/$USER/.gaustmp/$SLURM_JOBID
mkdir -p $GAUSS_SCRDIR

#Stop OpenMP from interfering with Gaussian's thread mechanism.
export OMP_NUM_THREADS=1

#Prepare node list for Linda
for n in `scontrol show hostname | sort -u`; do
  echo ${n}
done | paste -s -d, > snodes.$SLURM_JOBID
```

```
#Run Gaussian. It is recommended to only change the input file here. If needed you can
#raise the memory up to 60GB, but doing so may result in an error.
g16 -m=40gb -p=${SLURM_CPUS_PER_TASK} -w=`cat snodes.$SLURM_JOBID` silicene104.com

#Clean up nodes list
rm snodes.$SLURM_JOBID
```

Appendix C: Sample DOS Mathematica Code[silicene.nb]

```
data = Import["D:\\final_test\\dos\\snr\\silicene.dat"]

erg = 27.2 Flatten[Drop[data, 1]]

Homo = 27.2*(-0.16683)

Lumo = 27.2*(-0.15405)

-0.28287999999999996`
Ef = (Homo + Lumo)/2

\[Eta] = 25.0*10^-3;

S[x_] := Total[\[Eta]/(\[Eta]^2 + (x - erg)^2)];
Plot[S[x], {x, -8, -1}, PlotRange -> All, Frame -> True,
 Axes -> False, PlotStyle -> {Thick, Red}, GridLines -> {{Ef}, None},
 GridLinesStyle -> Directive[Gray, Dashed]]
```

Appendix D: Scholarly Presentations from this Research

1. **Mukesh Tumbapo** Matthew B. Henry,, and Benjamin O. Tayo, "Physisorption of DNA Bases on Nanoribbons from Graphene, Phosphorene and Silicene," 2020 Virtual Technical Meeting of the Oklahoma Academy of Sciences, November 6, 2020 (Contributor).
2. **Mukesh Tumbapo** and Benjamin O. Tayo, "DNA Sequencing Using Monolayer Silicene: A Computational Study," 2020 National Society of Black Physicists Virtual Meeting, Oral Presentation, November 7, 2020.
3. **Mukesh Tumbapo** and Benjamin O. Tayo, "Computational Studies of Monolayer Silicene for DNA Base Detection," 2020 Joint Texas APS Virtual meeting, Oral Presentation, Oral Presentation, November 13, 2020.
4. **Mukesh Tumbapo** and Benjamin O. Tayo, "First-Principle Studies of Silicene Nanostructures for DNA Base Detection," 2020 American Physical Society Virtual Meeting, Oral Presentation, March 15 - 19, 2021.
5. **Mukesh Tumbapo**, Matthew B. Henry, and Benjamin O. Tayo, "Phosphorene and Silicene Nanodevices for DNA Sequencing: Ab Initio Studies," 2020 American Physical Society Virtual Meeting, Oral Presentation, March 15 - 19, 2021 (Contributor).

Appendix E: Manuscripts from this Work

- **Mukesh Tumbapo**, Matthew B. Henry, and Benjamin O. Tayo, "Identification of DNA Bases Using Finite-Size Nanomaterials from Graphene, Phosphorene, and Silicene," (In Preparation)